

LOCKHEED MARTIN ENERGY RESEARCH LIBRARIES



3 4456 0514405 5

CENTRAL RESEARCH LIBRARY,  
DOCUMENT COLLECTION



**OAK RIDGE NATIONAL LABORATORY**

operated by

**UNION CARBIDE CORPORATION • NUCLEAR DIVISION**

for the

**U. S. ATOMIC ENERGY COMMISSION**



ORNL - TM - 3360

*copy 1*

OAK RIDGE NATIONAL LABORATORY SOLUTIONS  
TO A MODELING ROUND-ROBIN EXERCISE

F. J. Homan

OAK RIDGE NATIONAL LABORATORY  
CENTRAL RESEARCH LIBRARY  
DOCUMENT COLLECTION

**LIBRARY LOAN COPY**

DO NOT TRANSFER TO ANOTHER PERSON

If you wish someone else to see this document, send in name with document and the library will arrange a loan.

UCN-7969  
13 3-671

**NOTICE** This document contains information of a preliminary nature and was prepared primarily for internal use at the Oak Ridge National Laboratory. It is subject to revision or correction and therefore does not represent a final report.

This report was prepared as an account of work sponsored by the United States Government. Neither the United States nor the United States Atomic Energy Commission, nor any of their employees, nor any of their contractors, subcontractors, or their employees, makes any warranty, express or implied, or assumes any legal liability or responsibility for the accuracy, completeness or usefulness of any information, apparatus, product or process disclosed, or represents that its use would not infringe privately owned rights.

ORNL-TM-3360

Contract No. W-7405-eng-26

METALS AND CERAMICS DIVISION

OAK RIDGE NATIONAL LABORATORY SOLUTIONS  
TO A MODELING ROUND-ROBIN EXERCISE

F. J. Homan

AUGUST 1971

OAK RIDGE NATIONAL LABORATORY  
Oak Ridge, Tennessee  
operated by  
UNION CARBIDE CORPORATION  
for the  
U.S. ATOMIC ENERGY COMMISSION



3 4456 0514405 5



## CONTENTS

	<u>Page</u>
Abstract . . . . .	1
Introduction . . . . .	1
General Considerations . . . . .	2
Specific Data . . . . .	3
Predicted Performance . . . . .	10
Assumption . . . . .	10
Justification . . . . .	10
Assumption . . . . .	10
Justification . . . . .	10
Assumption . . . . .	17
Justification . . . . .	17
Discussion of Individual Pins . . . . .	18
F2Z . . . . .	18
F2H . . . . .	21
PNL 3-30 . . . . .	23
PNL 5-31 . . . . .	23
AI Demo . . . . .	24
MINT-2 . . . . .	25
Comments on the Comparison Between Predicted and Measured Performance . . . . .	27
Summary . . . . .	29
References . . . . .	30
Appendix A	
Data Supplied the Working Group for the Eight-Pin Round-Robin Exercise . . . . .	35
Annex I . . . . .	38
Appendix I . . . . .	49
Annex II . . . . .	54
Appendix II . . . . .	63
Annex III . . . . .	70
Annex IV . . . . .	72

100

•

•

•

•

•

•

OAK RIDGE NATIONAL LABORATORY SOLUTIONS  
TO A MODELING ROUND-ROBIN EXERCISE

F. J. Homan

ABSTRACT

Descriptions are given of eight problems included in a modeling round-robin exercise. Solutions to the problems obtained with the FMØDEL computer code are presented, with discussion of each individual pin. Assumptions made in obtaining the solutions are listed and discussed. Graphical and tabular comparisons between predicted performance and measured performance for two of the pins in the exercise are given and discussed. An appendix containing all the fabrication data and operating conditions provided the working group for this exercise is included.

---

INTRODUCTION

Early in 1969, a working group was established by the U.S. Atomic Energy Commission Division of Reactor Development and Technology to discuss and develop analytical techniques for predicting fuel pin performance. This group, which came to be known as the Working Group on Analytical Techniques for Predicting Fuel Pin Behavior and Design, met in March 1969 and again in April 1970. At the second meeting it was decided to select a number of fuel pins for analysis by each site participating in the working group. Eight fuel pins were selected for this "round-robin" exercise, and the data supplied to the working group for these pins are included in Appendix A of this report.

Using the data provided the working group and additional data from published sources, we analyzed the eight pins included in the exercise by means of the FMØDEL fuel performance computer code. The performance predictions resulting from analyses of the eight pins are included in this report. Also included are comparisons of predicted and measured performance parameters for pins that have undergone postirradiation examination.

## GENERAL CONSIDERATIONS

An up-to-date description of the computer code (FMØDEL) used to predict the performance of the eight pins included in the round-robin exercise does not exist. This model is not a production code but is undergoing continued development. We have been reporting our work on this code in two progress reports: The Fuels and Materials Development Program Quarterly Progress Report (beginning with the Period Ending September 30, 1969, ORNL-4480) and the monthly LMFBR Fuel Cycle Studies Progress Report (beginning with the report for March 1970, No. 13, ORNL-TM-2949). In addition, several items have been published in the open literature<sup>1-3</sup> dealing with work done with this code.

Two versions of the FMØDEL code are being developed simultaneously. The original version of the code<sup>1,2</sup> had only steady-state capabilities. It could consider up to 20 axial nodes, calculate fission-gas pressures and time-dependent temperature and stress distributions. But as our interests turned to transient, power cycling and other nonsteady-state modes of operation<sup>3</sup> we began to develop a version of the code that could be used to evaluate fuel-cladding mechanical interaction under conditions of rapidly changing reactor power. This version can only consider one axial node at a time, and time-dependent fission-gas pressures have to be input. We are now modifying our original multinode version for use in nonsteady-state situations, but it is not yet available for use with any degree of confidence. We expect to continue to develop both versions. The multinode version will be helpful for general analysis of a pin, while the single-node version will enable us to intensively study individual aspects of performance without great expense for computer time. Because the single-node version was used in the round-robin calculations, there will be no discussion of fission-gas pressures in the results presented later.

Detailed data on the individual pins in this exercise are included in Appendix A. General data and properties of fuel and cladding materials necessary for the analysis but not included in the data package have been taken from published sources. A summary of such data pertinent to the performance analysis of the eight pins and the sources of these data are shown in Table 1.

Table 1. Sources of Materials Data

	Reference Number
<u>Fuel Data</u>	
Thermal conductivity	4
Rupture modulus	5
Mechanical properties	6
Thermal expansion	7
Creep properties	8,9
Swelling characteristics	2,10
Restructuring characteristics	11
Formation of gas bubbles	12,13
<u>Cladding Data</u>	
Mechanical properties	14,15
Thermal expansion	16
Thermal creep equation	17
Void swelling	18
Irradiation-enhanced creep equation	19

## SPECIFIC DATA

The most important fabrication data and operating conditions for the eight pins considered in this round-robin exercise were extracted from Appendix A and are summarized in Tables 2-7. Note that although the eight pins were included in the study there are only six data tables, since two pins were modifications of other pins in the study. Two ratios of fluence to burnup were considered for PNL 5-31, and two smear densities were considered for the AI Demo pin. Table A2 in Appendix A very briefly summarizes the fabrication data and operating conditions of the eight pins.

Table 2. Fabrication Data and Operating Conditions for F2Z

Fabrication Data and Operating Conditions	Axial Region								
	1	2	3	4	5	6	7	8	9
Distance from bottom of fuel column, in.	0.79	2.37	3.94	5.52	7.10	8.68	10.26	11.83	13.41
	<u>Fabrication Data</u>								
Fuel pellet diameter, in.	0.2157	0.2159	0.2157	0.2160	0.2145	0.2151	0.2153	0.2153	0.2154
Fractional pellet density	0.893	0.893	0.893	0.893	0.893	0.893	0.893	0.893	0.893
Fuel cladding diametral gap, in.	0.0033	0.0031	0.0033	0.0030	0.0075	0.0039	0.0037	0.0037	0.0036
	<u>Type 316 Stainless Steel Cladding (Solution Annealed)</u>								
Cladding outside diameter, in.	0.249	0.249	0.249	0.249	0.249	0.249	0.249	0.249	0.249
Cladding thickness, in.	0.015	0.015	0.015	0.015	0.015	0.015	0.015	0.015	0.015
	<u>Operating Conditions</u>								
Heat rate, kW/ft	11.1	12.5	13.5	14.1	14.2	13.8	12.9	11.4	9.66
Flux, <sup>a</sup> neutrons cm <sup>-2</sup> sec <sup>-1</sup> ( > 0.1 MeV) × 10 <sup>-15</sup>	1.21	1.37	1.47	1.55	1.55	1.51	1.41	1.24	1.06
Fluence, <sup>a</sup> neutrons/cm <sup>2</sup> ( > 0.1 MeV) × 10 <sup>-22</sup>	2.16	2.43	2.62	2.76	2.76	2.68	2.51	2.21	1.88
Coolant temperature, °C	441	457	471	482	491	498	503	506	507
Fission rate, fissions cm <sup>-2</sup> sec <sup>-1</sup> × 10 <sup>-13</sup>	4.958	5.594	6.039	6.293	6.325	6.166	5.785	5.086	4.323
Power profile, region/peak	0.78	0.88	0.95	0.99	0.995	0.97	0.91	0.80	0.68

<sup>a</sup>See text for further discussion.

Table 3. Fabrication Data and Operating Conditions for F2H

Fabrication Data and Operating Conditions	Axial Region								
	1	2	3	4	5	6	7	8	9
Distance from bottom of fuel column, in.	0.79	2.37	3.94	5.52	7.10	8.68	10.26	11.83	13.41
	<u>Fabrication Data</u>								
Fuel pellet diameter, in.	0.2190	0.2186	0.2191	0.2188	0.2188	0.2176	0.2188	0.2188	0.2186
Fractional pellet density	0.953	0.953	0.953	0.953	0.953	0.953	0.953	0.953	0.953
Fuel cladding diametral gap, in.	0.0012	0.0016	0.0011	0.0014	0.0014	0.0026	0.0014	0.0014	0.0016
	<u>Type 316 Stainless Steel Cladding (Solution Anneal)</u>								
Cladding outside diameter, in.	0.249	0.249	0.249	0.249	0.249	0.249	0.249	0.249	0.249
Cladding thickness, in.	0.0144	0.0144	0.0144	0.0144	0.0144	0.0144	0.0144	0.0144	0.0144
	<u>Operating Conditions</u>								
Heat rate, kW/ft	11.9	13.3	14.5	15.1	15.1	14.6	13.6	12.2	10.3
Flux, <sup>a</sup> neutrons cm <sup>-2</sup> sec <sup>-1</sup> (> 0.1 MeV) × 10 <sup>-15</sup>	1.32	1.49	1.61	1.69	1.69	1.65	1.55	1.36	1.25
Fluence, <sup>a</sup> neutrons/cm <sup>2</sup> (> 0.1 MeV) × 10 <sup>-22</sup>	3.19	3.60	3.89	4.09	4.09	3.97	3.72	3.27	2.78
Coolant temperature, °C	443	463	471	497	499	507	513	516	518
Fission rate, fissions cm <sup>-2</sup> sec <sup>-1</sup> × 10 <sup>-13</sup>	4.958	5.594	6.039	6.293	6.325	6.166	5.785	5.086	4.323
Power profile, region/peak	0.78	0.88	0.95	0.99	0.995	0.97	0.91	0.80	0.68

<sup>a</sup>See text for further discussion.

Table 4. Fabrication Data and Operating Conditions for PNL 3-30

Fabrication Data and Operating Conditions	Axial Region								
	1	2	3	4	5	6	7	8	9
Distance from bottom of fuel column, in.	1.35	2.70	4.05	5.40	6.76	8.11	9.46	10.81	12.16
	<u>Fabrication Data</u>								
Fuel pellet diameter, in.	0.2136	0.2136	0.2136	0.2136	0.2136	0.2136	0.2136	0.2136	0.2136
Fractional pellet density	0.904	0.905	0.903	0.905	0.901	0.904	0.901	0.901	0.911
Fuel cladding diametral gap, in.	0.0057	0.0057	0.0057	0.0057	0.0057	0.0057	0.0057	0.0058	0.0056
	<u>Type 304 Stainless Steel Cladding (Solution Annealed)</u>								
Cladding outside diameter, in.	0.2505	0.2505	0.2505	0.2505	0.2505	0.2505	0.2505	0.2505	0.2505
Cladding thickness, in.	0.0156	0.0156	0.0156	0.0156	0.0156	0.0156	0.0156	0.0156	0.0156
	<u>Operating Conditions</u>								
Heat rate, <sup>a</sup> kW/ft	4.21	4.94	5.27	5.50	5.59	5.49	5.27	4.92	4.37
Flux, <sup>b</sup> neutrons cm <sup>-2</sup> sec <sup>-1</sup> (> 0.1 MeV) × 10 <sup>-15</sup>	1.35	1.50	1.62	1.69	1.71	1.69	1.62	1.50	1.35
Fluence, <sup>b</sup> neutrons/cm <sup>2</sup> (> 0.1 MeV) × 10 <sup>-22</sup>	3.61	4.02	4.34	4.52	4.57	4.52	4.34	4.02	3.61
Coolant temperature, °C	379	384	390	396	402	407	412	417	424
Fission rate, fissions cm <sup>-2</sup> sec <sup>-1</sup> × 10 <sup>-13</sup>	2.060	2.295	2.478	2.582	2.608	2.582	2.478	2.295	2.060
Power profile, region/peak	0.79	0.88	0.95	0.99	1.00	0.99	0.95	0.88	0.79

<sup>a</sup>Start of life.<sup>b</sup>See text for further discussion.

Table 5. Fabrication Data and Operating Conditions for PNL 5-31

Fabrication Data and Operating Conditions	Axial Region								
	1	2	3	4	5	6	7	8	9
Distance from bottom of fuel column, in.	1.35	2.07	4.05	5.40	6.76	8.11	9.46	10.81	12.16
	<u>Fabrication Data</u>								
Fuel pellet diameter, in.	0.2137	0.2136	0.2135	0.2136	0.2136	0.2135	0.2136	0.2135	0.2135
Fractional pellet density	0.914	0.913	0.911	0.911	0.916	0.913	0.913	0.911	0.915
Fuel cladding diametral gap, in.	0.0059	0.0060	0.0061	0.0061	0.0060	0.0061	0.0060	0.0061	0.0061
	<u>Type 304 Stainless Steel Cladding (Solution Annealed)</u>								
Cladding outside diameter, in.	0.2504	0.2504	0.2504	0.2504	0.2504	0.2504	0.2504	0.2504	0.2504
Cladding thickness, in.	0.0154	0.0154	0.0154	0.0154	0.0154	0.0154	0.0154	0.0154	0.0154
	<u>Operating Conditions</u>								
Heat rate, <sup>a</sup> kW/ft	11.49	12.92	13.93	14.48	14.69	14.47	13.85	12.90	11.58
Flux, <sup>b</sup> neutrons cm <sup>-2</sup> sec <sup>-1</sup> (> 0.1 MeV) × 10 <sup>-15</sup>	1.15/ 3.55	1.29/ 4.00	1.40/ 4.32	1.46/ 4.50	1.47/ 4.55	1.46/ 4.50	1.40/ 4.28	1.29/ 7.70	1.15/ 3.59
Fluence, <sup>b</sup> neutrons/cm <sup>2</sup> (> 0.1 MeV) × 10 <sup>-22</sup>	2.25/ 6.83	2.53/ 7.70	2.74/ 8.31	2.85/ 8.66	2.88/ 8.75	2.85/ 8.66	2.74/ 8.31	2.53/ 7.70	2.25/ 6.83
Coolant temperature, °C	392	407	421	436	450	466	479	487	502
Fission rate, fissions cm <sup>-2</sup> sec <sup>-1</sup> × 10 <sup>-13</sup>	5.34	6.03	6.51	6.78	6.85	6.78	6.51	6.03	5.34
Power profile, region/peak	0.78	0.88	0.95	0.99	1.00	0.99	0.94	0.88	0.79

<sup>a</sup>Start of life.<sup>b</sup>PNL/PNL modified.

Table 6. Fabrication Data and Operating Conditions for AI Demo Pin

Fabrication Data and Operating Conditions	Axial Region								
	1	2	3	4	5	6	7	8	9
Distance from bottom of fuel column, in.	5.11	10.22	15.33	20.44	25.55	30.66	35.77	40.88	45.99
	<u>Fabrication Data</u>								
Fuel pellet diameter, in.	0.2580	0.2580	0.2580	0.2580	0.2580	0.2580	0.2580	0.2580	0.2580
Fractional pellet density <sup>a</sup>	0.838/ 0.890	0.838/ 0.890	0.838/ 0.890	0.838/ 0.890	0.838/ 0.890	0.838/ 0.890	0.838/ 0.890	0.838/ 0.890	0.838/ 0.890
Fuel cladding diametral gap, in.	0.006	0.006	0.006	0.006	0.006	0.006	0.006	0.006	0.006
	<u>Type 316 Stainless Steel Cladding (20% Cold Worked)</u>								
Cladding outside diameter, in.	0.300	0.300	0.300	0.300	0.300	0.300	0.300	0.300	0.300
Cladding thickness, in.	0.018	0.018	0.018	0.018	0.018	0.018	0.018	0.018	0.018
	<u>Operating Conditions</u>								
Heat rate, kW/ft	7.6	10.9	13.2	14.5	15.0	14.5	13.2	10.9	7.6
Flux, <sup>b</sup> neutrons cm <sup>-2</sup> sec <sup>-1</sup> (> 0.1 MeV) × 10 <sup>-15</sup>	3.40	4.87	5.87	6.47	6.67	6.47	5.87	4.87	3.40
Fluence, <sup>b</sup> neutrons/cm <sup>2</sup> (> 0.1 MeV) × 10 <sup>-23</sup>	1.58	2.26	2.73	3.01	3.10	3.01	2.73	2.26	1.58
Coolant temperature, °C	423	441	464	487	511	535	556	573	585
Fission rate, fissions cm <sup>-2</sup> sec <sup>-1</sup> × 10 <sup>-13</sup>	2.444	3.500	4.218	4.649	4.793	4.649	4.218	3.500	2.444
Power profile, region/peak	0.51	0.73	0.88	0.97	1.00	0.97	0.88	0.73	0.51

<sup>a</sup>80% smear density/85% smear density.

<sup>b</sup>See text for further discussion.

Table 7. Fabrication Data and Operating Conditions for MINT-2

Fabrication Data and Operating Conditions	Axial Region								
	1	2	3	4	5	6	7	8	9
Distance from bottom of fuel column, in.	0.96	1.92	2.88	3.84	4.80	5.76	6.72	7.68	8.64
	<u>Fabrication Data</u>								
Fuel pellet diameter, in.	0.198	0.198	0.198	0.198	0.198	0.198	0.198	0.198	0.198
Fractional pellet density	0.920	0.920	0.920	0.920	0.920	0.920	0.920	0.920	0.920
Fuel cladding diametral gap, in.	0.002	0.002	0.002	0.002	0.002	0.002	0.002	0.002	0.002
	<u>Type 316 Stainless Steel Cladding (20% Cold Worked)</u>								
Cladding outside diameter, in.	0.230	0.230	0.230	0.230	0.230	0.230	0.230	0.230	0.230
Cladding thickness, in.	0.015	0.015	0.015	0.015	0.015	0.015	0.015	0.015	0.015
	<u>Operating Conditions</u>								
Heat rate, <sup>a</sup> kW/ft	13.6	14.3	15.0	15.7	16.0	15.7	15.0	14.3	13.6
Flux, <sup>b</sup> neutrons cm <sup>-2</sup> sec <sup>-1</sup> (> 0.1 MeV) × 10 <sup>-15</sup>									
Fluence, <sup>b</sup> neutrons/cm <sup>2</sup> (> 0.1 MeV) × 10 <sup>-23</sup>									
Coolant temperature, °C	535	559	581	604	615	604	581	559	535
Fission rate, fissions cm <sup>-2</sup> sec <sup>-1</sup> × 10 <sup>-13</sup>	7.176	7.556	7.919	8.273	8.442	8.273	7.919	7.556	7.176
Power profile, region/peak	0.850	0.895	0.938	0.980	1.00	0.980	0.938	0.895	0.850

<sup>a</sup>See text for further discussion.

<sup>b</sup>Fast flux and fluence are too low to be of importance in cladding swelling.

## PREDICTED PERFORMANCE

A summary of the predicted performance of the eight pins in this exercise is tabulated in Tables 8-13. Most entries in the tables represent end-of-life conditions. Additional performance information is contained in the next section of this report, where each pin is discussed individually.

In interpreting the information contained in Tables 8-13, one should be aware of several assumptions built into the FM~~ODEL~~ code. A summary of these assumptions and justification for each are included below.

### Assumption

The heat transfer coefficient across the fuel-cladding gap is constant and equal to  $1.14 \text{ W cm}^{-2} \text{ }^{\circ}\text{C}^{-1}$ .

### Justification

The constant heat transfer coefficient is used because we have not yet built into the code a good model for varying heat transfer coefficient with changing gap size and gas composition. The value of  $1.14 \text{ W cm}^{-2} \text{ }^{\circ}\text{C}^{-1}$  is appropriate for pellets with a 2-mil diametral gap and for initial gaps as large as 6 mils after several weeks of irradiation.<sup>4</sup> Using this value, we have obtained good agreement between predicted and measured fuel temperatures.<sup>20,21</sup>

### Assumption

Cladding mechanical properties and creep strengths change only with temperature.

### Justification

It is well known that annealed claddings harden and cold-worked claddings soften with fast-neutron exposure. However, good quantitative

Table 8. Predicted Performance for F2Z

Predicted Performance	Axial Region								
	1	2	3	4	5	6	7	8	9
Temperature, °C									
Fuel surface	683	729	763	789	797	795	782	751	716
Fuel center	1930	2065	2176	2274	2257	2224	2140	1992	1881
Diameter, in.									
Void	0.0354	0.0444	0.0474	0.0484	0.0486	0.0485	0.0470	0.0414	0.0238
Columnar grain	None	0.1214	0.1389	0.1469	0.1460	0.1464	0.1464	0.1109	None
Equiaxed grain	0.1674	0.1747	0.1745	0.1811	0.1799	0.1806	0.1808	0.1740	0.1599
Fission product swelling, % $\Delta V/V$	0.125	0.445	0.640	0.794	0.786	0.731	0.584	0.284	0
Burnup, % FIMA	3.87	4.30	4.61	4.83	4.83	4.69	4.43	3.93	3.43
Maximum mechanical inter- action, psi	No fuel cladding mechanical interaction predicted								
Cladding plastic strain, <sup>a</sup> %	0.0244	0.0269	0.0278	0.0282	0.0269	0.0253	0.0229	0.0189	0.0148
Cladding swelling, <sup>a</sup> % $\Delta V/V$	0.721	0.935	1.09	1.19	1.19	1.12	0.996	0.798	0.606
Maximum cladding hoop stress, <sup>a</sup> psi	18,559	19,002	20,162	21,274	21,019	20,538	19,318	17,004	14,497
Predicted cladding $\Delta D$ , mils (at 25°C)	0.74	0.91	1.02	1.09	1.07	1.01	0.91	0.75	0.60
Measured cladding $\Delta D$ , <sup>b</sup> mils	0.6-0.8	0.8-1.1	1.0-1.3	0.7-1.5	0.7-2.0	1.0-1.7	0.8-1.8	0.5-1.0	0.4-0.8
Maximum cladding hot strain, % $\Delta D/D$	1.21	1.33	1.42	1.48	1.50	1.49	1.46	1.39	1.10

<sup>a</sup>Calculated at cladding outer surface.

<sup>b</sup>Range represents 0 and 90° orientation of postirradiation profilometer trace.

Table 9. Predicted Performance for F2H

Predicted Performance	Axial Region								
	1	2	3	4	5	6	7	8	9
Temperature, °C									
Fuel surface	689	738	768	808	810	806	796	766	730
Fuel center	1896	2065	2219	2342	2344	2231	2194	1986	1774
Diameter, in.									
Void	0.00337	0.0192	0.0215	0.0241	0.0243	0.0302	0.0206	0.0178	0.00617
Columnar grain	None	0.1097	0.1300	0.1474	0.1431	0.1395	0.1297	0.0982	None
Equiaxed grain	0.1556	0.1703	0.1776	0.1842	0.1842	0.1843	0.1840	0.1704	0.1558
Fission product swelling, % $\Delta V/V$	2.91	3.38	3.56	3.74	3.73	3.66	3.39	2.96	2.53
Burnup, % FIMA	5.07	5.65	6.08	6.39	6.38	6.20	5.82	5.15	4.42
Maximum mechanical inter- action, psi	382	382	3200	2400	2400	None	800	770	None
Cladding plastic strain, <sup>a</sup> %	0.0424	1.0124	0.254	0.189	0.190	0.414	0.0513	0.0336	0.0224
Cladding swelling, <sup>a</sup> % $\Delta V/V$	1.44	1.88	2.16	2.33	2.33	2.18	1.94	1.55	1.17
Maximum cladding hoop stress, <sup>a</sup> psi	17,147	13,984	27,111	21,445	21,427	13,099	14,076	12,841	12,776
Predicted cladding, $\Delta D$ , <sup>b</sup> mils (at 25°C)	1.29	1.60	2.29	2.20	2.30	1.74	1.56	1.25	0.96
Measured cladding, $\Delta D$ , <sup>c</sup> mils	1.5-1.5	2.5-2.6	2.8-2.8	2.8-3.4	2.3-3.3	2.0-3.0	1.4-2.7	0.7-2.0	0-1.0
Maximum cladding hot strain, <sup>b</sup> % $\Delta D/D$	1.47	1.66	1.97	2.01	2.02	1.85	1.79	1.66	1.53

<sup>a</sup>Calculated at cladding outer surface.

<sup>b</sup>Reflects peak fast fluence of  $4.09 \times 10^{22}$  neutrons/cm<sup>2</sup>.

<sup>c</sup>Range represents 0 and 90° orientation of postirradiation profilometer.

Table 10. Predicted Performance for PNL 3-30

Predicted Performance	Axial Region								
	1	2	3	4	5	6	7	8	9
Temperature, °C									
Fuel surface	471	486	499	510	517	520	520	518	515
Fuel center	823	889	949	985	1010	1003	983	941	875
Diameter, in.									
Void									
Columnar grain	No fuel restructuring predicted								
Equiaxed grain	No fuel restructuring predicted								
Fission product swelling, % $\Delta V/V$	0	0	0	0	0	0	0	0	0
Burnup, % FIMA	2.38	2.64	2.84	2.97	3.02	2.98	2.86	2.65	2.36
Maximum mechanical inter- action, psi	No fuel cladding mechanical interaction predicted								
Cladding plastic strain, <sup>a</sup> % $\times 10^{-3}$	9.12	1.16	1.36	1.46	1.43	1.34	1.15	9.24	6.80
Cladding swelling, <sup>a</sup> % $\Delta V/V$	0.884	1.15	1.41	1.64	1.78	1.83	1.78	1.62	1.42
Maximum cladding hoop stress, <sup>a</sup> psi	6147	7456	8437	8923	8778	8297	7351	6167	4844
Predicted cladding $\Delta D$ , mils (at 25°C)	0.930	1.18	1.42	1.62	1.73	1.77	1.70	1.55	1.35
Measured cladding $\Delta D$ , mils	No measured values included in data package								
Maximum cladding hot strain, % $\Delta D/D$	1.03	1.14	1.25	1.34	1.40	1.42	1.41	1.35	1.29

<sup>a</sup>Calculated at cladding outer surface.

Table 11. Predicted Performance for PNL 5-31

Predicted Performance	Axial Region								
	1	2	3	4	5	6	7	8	9
Temperature, °C									
Fuel surface	626	671	703	730	746	758	758	747	730
Fuel center	1756	1885	1985	2071	2105	2104	2054	1966	1822
Diameter, in.									
Void	0.0234	0.0364	0.0408	0.0421	0.0406	0.0416	0.0412	0.0400	0.0339
Columnar grain	None	0.1094	0.1287	0.1371	0.1371	0.1371	0.1370	0.1198	0.0934
Equiaxed grain	0.1514	0.1662	0.1731	0.1730	0.1730	0.1728	0.1730	0.1729	0.1660
Fission product swelling, % $\Delta V/V$	0.176	0.612	0.882	0.971	1.05	1.02	0.867	0.704	0.432
Burnup, % FIMA	4.36	4.86	5.20	5.41	5.44	5.39	5.15	4.84	4.32
Maximum mechanical inter- action, psi	No fuel cladding mechanical interaction predicted								
Cladding plastic strain, <sup>a</sup> %	0.0123- 0.144	0.0142- 0.169	0.0147- 0.137	0.0142- 0.0698	0.0130- 0.0469	0.0114- 0.0306	0.00986- 0.0209	0.0086- 0.0170	0.0068- 0.0126
Cladding swelling, <sup>a</sup> % $\Delta V/V$	0.504- 3.48	0.730- 5.03	0.919- 6.33	1.07- 7.37	1.14- 7.86	1.15- 7.95	1.07- 7.38	0.951- 6.56	0.768- 5.30
Maximum cladding hoop stress, <sup>a</sup> psi	12,228- 30,433	12,935- 32,458	12,609- 29,453	11,558- 22,674	10,268- 15,082	8,858- 7,118	7,957- 2,717	7,536- 1,619	6,962- 651
Predicted cladding $\Delta D$ , <sup>b</sup> mils (at 25°C)	0.613- 3.61	0.809- 4.97	0.958- 5.98	1.06- 6.67	1.09- 6.89	1.07- 6.77	0.989- 6.19	0.886- 5.48	0.729- 4.41
Measured cladding $\Delta D$ , mils	No measured values included in data package								
Maximum cladding hot strain, <sup>b</sup> % $\Delta D/D$	0.990- 2.18	1.11- 2.76	1.20- 3.20	1.27- 3.51	1.32- 3.63	1.34- 3.62	1.33- 3.40	1.30- 3.13	1.26- 2.73

<sup>a</sup>Calculated at cladding outer surface.

<sup>b</sup>A/B: A = calculations for PNL 5-31; B = calculations for PNL 5-31 (modified).

Table 12. Predicted Performance for AI Demo Pin

Predicted Performance	Axial Region								
	1	2	3	4	5	6	7	8	9
Temperature, <sup>a</sup> °C									
Fuel surface	568	647	711	758	790	805	801	776	727
Fuel center	1558-1429	1868-1843	2063-2059	2252-2295	2570-2393	2348-2377	2135-2153	1948-1959	1759-1671
Diameter, <sup>a</sup> in.									
Void	0.00104-none	0.0601-0.0417	0.0722-0.0522	0.0696-0.0487	0.0374-0.0457	0.0629-0.0439	0.0745-0.0567	0.0687-0.0518	0.0218-0.00609
Columnar grain	None-none	0.1230-none	0.1684-0.1662	0.1840-0.1732	0.1822-0.1976	0.1894-0.1804	0.1858-0.7664	0.1580-0.1450	None-none
Equiaxed grain	0.0816-none	0.1744-0.1536	0.202-0.1844	0.208-0.1988	0.206-0.214	0.204-0.206	0.210-0.1938	0.1930-0.1838	0.1292-0.1290
Fission product swelling, <sup>a</sup> % ΔV/V	0-0	0.609-0.52	1.41-1.58	1.94-2.37	2.24-2.71	2.11-2.47	1.63-1.79	0.926-0.944	0-0
Burnup, <sup>a</sup> % FIMA	5.53-5.21	7.51-7.26	8.80-8.57	9.56-9.34	9.75-9.58	9.50-9.30	8.72-8.51	7.38-7.16	5.49-5.20
Maximum mechanical interaction, psi	No fuel cladding mechanical interaction predicted								
Cladding plastic strain, <sup>b</sup> %	0.122	0.248	0.351	0.376	0.304	0.189	0.106	0.061	0.039
Cladding swelling, <sup>b</sup> % ΔV/V	3.26	6.93	11.16	14.9	17.4	17.8	15.9	12.2	7.14
Maximum cladding hoop stress, <sup>b</sup> psi	19,582	32,110	36,896	35,708	30,345	20,707	10,814	5,843	5,728
Predicted cladding ΔD, mils (at 25°C)	4.00	8.34	13.0	16.8	18.9	18.7	16.4	12.4	7.31
Measured cladding ΔD, mils	No measured values included in data package								
Maximum cladding hot strain, <sup>b</sup> % ΔD/D	2.35	3.62	5.22	6.54	7.30	7.30	6.56	5.26	3.57

<sup>a</sup>A/B; A = 80% smear density; B = 85% smear density.

<sup>b</sup>Calculated at cladding outer surface.

5

Table 13. Predicted Performance for MINT-2

Predicted Performance	Axial Region								
	1	2	3	4	5	6	7	8	9
Temperature, °C									
Fuel surface	825		900		953				
Fuel center	2207		2447		2606				
Diameter, in.									
Void	0.0288		0.0295		0.0287				
Columnar grain	0.1325		0.1524		0.1584				
Equiaxed grain	0.1650		0.1816		0.1814				
Fission product swelling, % $\Delta V/V$	2.44		2.97		3.36				
Burnup, % FIMA	6.70		7.31		7.79				
Maximum mechanical inter- action, psi	462		416		457				
Cladding plastic strain, <sup>a</sup> %	1.15 $\times 10^{-4}$		2.59 $\times 10^{-4}$		1.32 $\times 10^{-3}$				
Cladding swelling, <sup>a</sup> % $\Delta V/V$	Negligible cladding swelling due to irradiation in a thermal flux								
Maximum cladding hoop stress, <sup>a</sup> psi	9067		9119		8897				
Predicted cladding $\Delta D$ , mils (at 25°C)	0.094		0.094		0.094				
Measured cladding $\Delta D$ , mils	No measured values included in data package								
Maximum cladding hot strain, % $\Delta D/D$	1.05		1.15		1.22				

<sup>a</sup>Calculated at cladding outer surface.

descriptions of the change in mechanical properties and creep strengths with neutron exposure over the temperature and stress ranges of interest are not available. The error associated with failure to consider such changes in properties would be greatest in situations where cladding stresses are high, such as during fuel-cladding mechanical interaction. Mechanical interaction was predicted for two of the pins in this study - F2H and MINT-2. In the case of F2H, the major interaction was due to differential thermal expansion during startup, and very little fast-neutron exposure had been experienced by the cladding at that point. Therefore, the assumption being discussed here is valid for that pin. For MINT-2, however, mechanical interactions were predicted throughout the life of the pin. But this pin will be irradiated in a thermal flux, where the changes in properties will be much reduced. The assumption is, therefore, reasonable for this pin also.

#### Assumption

The creep characteristics of the fuel material can adequately be described by out-of-reactor data for  $UO_2$ .

#### Justification

Again, it is known qualitatively that mixed oxide fuels under irradiation creep more rapidly due to fissioning than  $UO_2$  out-of-reactor when exposed to the same temperatures and stresses. Bohaboy<sup>22</sup> has suggested a creep rate increased by a factor of 4 to 5 due to the replacement of uranium atoms by plutonium atoms in the mixed oxide lattice, and Perrin et al.<sup>23</sup> have suggested a factor of 8 to 10 increase in the  $1100^\circ C$  creep rate of  $UO_2$  in-reactor compared to out-of-reactor. All of this notwithstanding, it is difficult to use such qualitative information in a mathematical model. The fuel creep equations<sup>8,9</sup> that are employed in FMODEL cover the entire stress, temperature, and porosity regions of interest. Creep expressions of this type for mixed oxide fuels under irradiation conditions are simply not available. The creep law employed becomes important in FMODEL only when there is fuel-cladding mechanical

interaction. A weaker fuel would result in a less severe interaction. As indicated before, only F2H and MINT-2 are predicted to experience fuel-cladding mechanical interaction; therefore, it is possible that there are significant errors in the interactions predicted for these pins through use of this assumption, but no errors have been introduced into the other six pins in the exercise.

#### DISCUSSION OF INDIVIDUAL PINS

##### F2Z

An apparent inconsistency was noted in the preirradiation data contained in the data package for this pin. Table I.5 of the data package indicates that the largest pellet (18) and the smallest pellet (29) had as-fabricated diameters of 0.2180 and 0.2160 in., respectively. These data yield a range of 0.8 to 2.8 mils for the cold fuel-cladding diametral gap. This value for the gap range does not agree with the 2.1- to 4.8-mils gap range listed on p. 45 of the data package or the 2.3- to 4.3-mils gap range reported in the literature.<sup>24</sup> We resolved the inconsistency by assuming the gap sizes reported in the literature<sup>24</sup> were correct and calculating pellet diameters that would be in agreement. A summary of these diameters is included in Table 14.

Other apparent inconsistencies in the data given for this pin involved the neutron flux and fluence listed on the summary page of the data package and the total number of effective full power days (EFPD) given on p. 42 of the package. This problem was also noted with several other pins in the round-robin exercise. According to the data package, F2Z operated for 207.1 EFPD at a peak total neutron flux of  $2.07 \times 10^{15}$  neutrons  $\text{cm}^{-2} \text{sec}^{-1}$ . This flux would yield a peak total neutron fluence of  $3.70 \times 10^{22}$  neutrons/ $\text{cm}^2$ ; but the total fluence reported in the summary sheet of the data package is  $4.18 \times 10^{22}$  neutrons/ $\text{cm}^2$ . To achieve this latter fluence, a total flux of  $2.34 \times 10^{15}$  neutrons  $\text{cm}^{-2} \text{sec}^{-1}$  over 207.1 EFPD would be required. This difficulty was resolved by assuming that the EFPD figure is correct and running the case with both of the neutron fluxes given above. The resulting predictions for

Table 14. Pellet Diameter<sup>a</sup> and Gap Data  
for Nine Axial Regions of GE Pin F2Z

Axial Location ( $l/L$ )	Pellet Diameter, in.		Average Diametral Gap <sup>c</sup> (in.)	Calculated Average Pellet Diameter (in.)
	Maximum <sup>b</sup>	Average <sup>b</sup>		
0.050	0.2175	0.2171	0.0031	0.2157
0.167	0.2178	0.2173	0.0029	0.2159
0.227	0.2180	0.2172	0.0031	0.2157
0.389	0.2179	0.2176	0.0028	0.2160
0.500	0.2169	0.2164	0.0043	0.2145
0.611	0.2170	0.2169	0.0037	0.2151
0.723	0.2172	0.2171	0.0035	0.2153
0.833	0.2172	0.2171	0.0035	0.2153
0.944	0.2175	0.2173	0.0034	0.2154

<sup>a</sup>All diameters reflect the pellets in an axial region of length  $l/q$  and midpoint  $l/L$ .

<sup>b</sup>As given in Table I.5 of data package.

<sup>c</sup>As given in GEAP-13549, pp. 93-94.

cladding swelling, diametral expansion, and plastic strain are tabulated in Table 15. Total fluxes were converted to fast fluxes by using the conversion factor of 0.739 suggested in the data package (see Appendix A, p. 42).

Figure 1 is a plot of the predicted cladding diametral expansion values at each of the nine axial nodes superimposed on the postirradiation profilometer traces reported in the literature.<sup>25</sup> The predicted values represent the lower flux and fluence numbers mentioned earlier. The postirradiation data given on p. 46 of Appendix A show the void diameter and columnar grain region diameter as 0.0465 and 0.1434 in., respectively, for a transverse section 6.52 in. from the bottom of the pin. The predicted values for these quantities are 0.0484 and 0.1460 in., respectively.

Table 15. Predicted Performance at Different Neutron Exposures for F2Z

Axial Location ( <i>l</i> /L)	Cladding $\Delta D$ , mils				Predicted Cladding			
	Measured		Predicted		Plastic Strain (%)		Swelling (% $\Delta V/V$ )	
	0°	90°	A	B	A	B	A	B
	$\times 10^{-2}$							
0.056	0.8	0.6	0.896	0.707	2.75	$2.44 \times 10^{-2}$	0.889	0.721
0.167	1.1	0.8	1.10	0.910	3.00	$2.69 \times 10^{-2}$	1.15	0.935
0.277	1.3	1.0	1.23	1.02	3.05	$2.78 \times 10^{-2}$	1.34	1.09
0.389	1.5	0.7	1.31	1.08	3.06	$2.82 \times 10^{-2}$	1.46	1.19
0.500	2.0	0.7	1.29	1.06	2.88	$2.69 \times 10^{-2}$	1.46	1.19
0.611	1.7	1.0	1.21	1.00	2.70	$2.53 \times 10^{-2}$	1.38	1.12
0.723	1.8	0.8	1.09	0.906	2.45	$2.29 \times 10^{-2}$	1.23	0.996
0.833	1.0	0.5	0.902	0.752	2.05	$1.89 \times 10^{-2}$	0.985	0.798
0.944	0.8	0.4	0.716	0.601	1.62	$1.48 \times 10^{-3}$	0.748	0.606

	A	B
Key: Peak fast flux, neutrons $\text{cm}^{-2} \text{sec}^{-1} \times 10^{-15}$	1.73	1.53
Peak fast fluence, neutrons/ $\text{cm}^2 \times 10^{-22}$	3.10	2.73

ORNL-DWG 71-915R

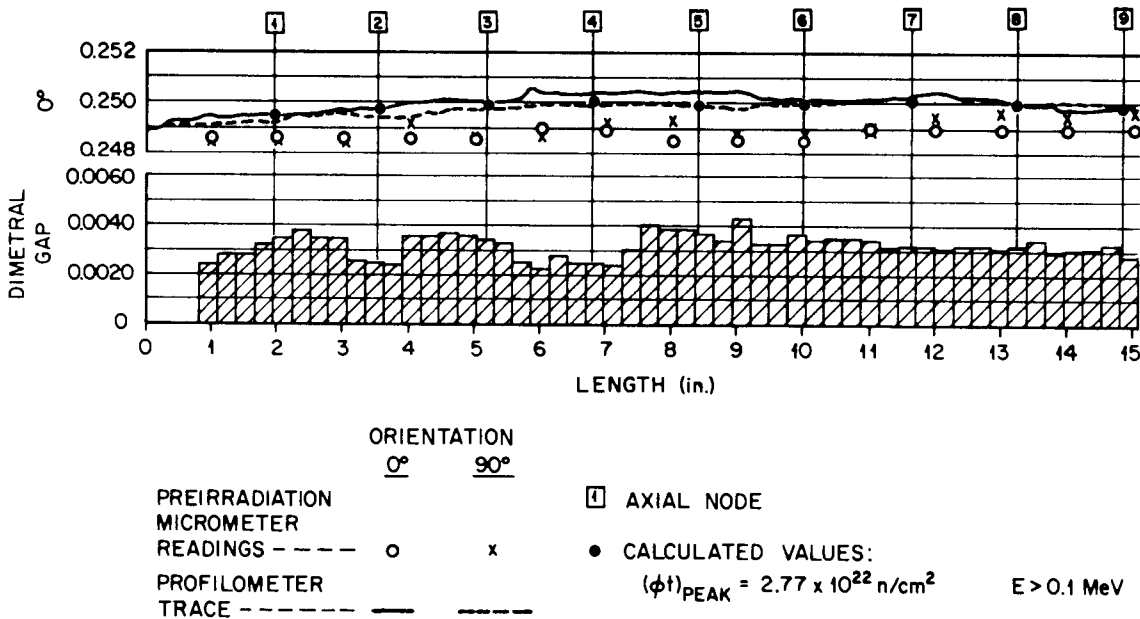


Fig. 1. Comparison of Predicted and Measured Diametral Expansions for Pin F2Z.

## F2H

Difficulty was encountered in selecting the proper as-fabricated pellet diameters for the analysis of this pin. Table I.4 of the data package lists the fabricated pellet diameters, and examination of that table reveals that the difference between the diameters of the largest and smallest pellets is 3.6 mils. This is nearly twice the difference noted for F2Z. Graphical representation of the variation in pellet diameter with axial position for this pin is available in the literature.<sup>26</sup> The problem concerns the fact that dividing the pin into nine axial regions results in about nine pellets per region. The question now is what pellet diameter to use in the model to represent the fuel within that region. Should it be the average diameter, the diameter of the largest pellet, or the diameter of the pellet nearest the midpoint of the region? This problem was investigated in more detail recently,<sup>27</sup> and for purposes of this round-robin exercise we have chosen the maximum (for the region) pellet diameter as representative of the fuel in a given axial region. This problem also existed for F2Z, but to a lesser degree. With that pin, the choice was not nearly as critical because no fuel-cladding mechanical interaction during startup was predicted for any choice of pellet diameters. But with F2H, mechanical interaction during startup is predicted at axial nodes 3, 4, 5, and 7. Additional mechanical interaction due to fuel swelling is predicted at these nodes and also at nodes 1, 2, and 8. The magnitude of the mechanical interaction is strongly influenced by the size of the fuel-cladding gap (or size of the as-fabricated fuel pellets). The study referenced earlier<sup>27</sup> explores this difficulty in great detail; it will not be discussed further here except to note that the fluence used in the earlier study is somewhat higher than reported in the round-robin data package, resulting in slightly more cladding swelling than in the calculations presented here.

The same difficulty with the neutron flux and fluence values given on the summary page of the data package (and covered in the discussion on F2Z) was encountered with this pin. The difficulty was resolved in the same manner as with F2Z. The calculations tabulated in Table 9, p. 12,

reflect a peak fast neutron flux of  $1.69 \times 10^{15}$  neutrons  $\text{cm}^{-2} \text{sec}^{-1}$ . Table 16 presents the predicted performance at both flux levels and the measured diametral expansion for this pin.

Table 16. Predicted Performance at Different Neutron Exposures for F2H

Axial Location ( $l/L$ )	Cladding $\Delta D$ , mils				Predicted Cladding			
	Measured		Predicted		Plastic Strain (%)		Swelling (% $\Delta V/V$ )	
	0°	90°	A	B	A	B	A	B
0.056	1.5	1.5	1.29	1.09	$4.24 \times 10^{-2}$	$3.91 \times 10^{-2}$	1.44	1.22
0.167	2.6	2.5	1.60	1.36	$4.60 \times 10^{-2}$	$4.36 \times 10^{-2}$	1.88	1.58
0.277	2.8	2.8	2.29	2.01	$2.54 \times 10^{-1}$	$2.53 \times 10^{-1}$	2.16	1.82
0.389	3.4	2.8	2.20	1.91	$1.89 \times 10^{-1}$	$1.90 \times 10^{-1}$	2.33	1.97
0.500	3.3	2.3	2.30	1.91	$1.90 \times 10^{-1}$	$1.91 \times 10^{-1}$	2.33	1.96
0.611	3.0	2.0	1.74	1.48	$4.14 \times 10^{-2}$	$4.30 \times 10^{-2}$	2.18	1.84
0.723	2.7	1.4	1.56	1.32	$5.13 \times 10^{-2}$	$5.19 \times 10^{-2}$	1.94	1.63
0.833	2.0	0.7	1.25	1.06	$3.36 \times 10^{-2}$	$3.28 \times 10^{-2}$	1.55	1.31
0.944	1.0	0	0.959		$2.24 \times 10^{-2}$		1.17	
Key:					A	B		
Peak fast flux, neutrons $\text{cm}^{-2} \text{sec}^{-1} \times 10^{-15}$					1.69	1.53		
Peak fast fluence, neutrons/ $\text{cm}^2 \times 10^{-22}$					4.09	3.70		

A comparison between predicted and measured cladding diametral expansion for F2H is presented in Fig. 2. The postirradiation profilometer traces were taken from Baily.<sup>26</sup> As indicated on the figure, predicted points were plotted from both the fast flux values that could have been derived from the summary page of the data package. Postirradiation data given on p. 46 of Appendix A show the void diameter and diameters of the columnar and equiaxed grain regions as 0.0109, 0.1027, and 0.1605 in., respectively, for a transverse section 11.86 in. from the bottom of the pin. The predicted values for these quantities are 0.0178, 0.0982, and 0.1704 in., respectively.

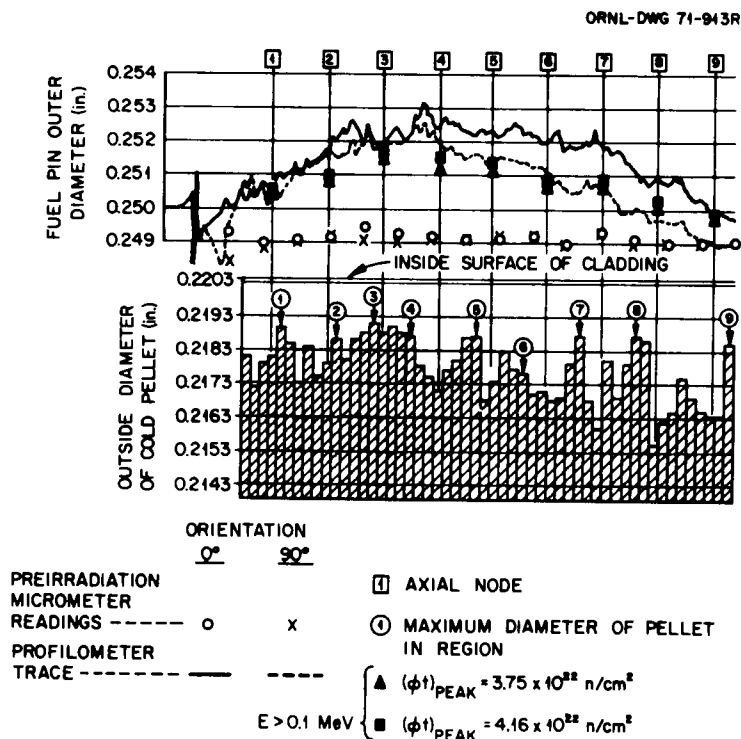


Fig. 2. Comparison of Predicted and Measured Diametral Expansions for Pin F2H.

PNL 3-30

This pin was operated at a low heat rate and began life with a large fuel-cladding diametral gap. No fuel restructuring is predicted. The data package indicates that the peak heat rate decreases from 5.59 to 5.20 kW/ft during the operating lifetime of this pin. We have assumed that the decrease in power is a linear function of time.

PNL 5-31

Two fluence/burnup conditions are considered in this problem. The higher fluence/burnup case (designated PNL 5-31 modified) exhibits considerably greater cladding swelling than the lower ratio case, as expected. As with PNL 3-30, a decrease in the peak heat rate occurs during the operating lifetime of this pin. This decrease is given in the data package as from 14.7 kW/ft at the beginning of life to 13.7 kW/ft at the end of life. We have assumed that the decrease is a linear function of time.

The Westinghouse-PNL cladding swelling equations<sup>18</sup> are based on swelling data to  $7 \times 10^{22}$  neutrons/cm<sup>2</sup> fast fluence. Examination of Table 5, p. 7, reveals that for PNL 5-31 (modified) the cladding fast fluence values at most axial positions studied are somewhat above  $7 \times 10^{22}$  neutrons/cm<sup>2</sup>. It is our opinion that the Westinghouse-PNL equations cannot be extrapolated. Therefore we attach little meaning to the cladding performance predictions for PNL 5-31 (modified) that are listed in Table 11, p. 14.

#### AI Demo

This problem is also composed of two parts, an 80% smear density case and an 85% smear density case. Unlike the PNL 5-31 problem, there is no difference in cladding performance between the two cases. There are some differences in fuel performance, however, and these differences are noted in Table 12, p. 15. The fast-fluence values listed in Table 6, p. 8, are considerably above  $7 \times 10^{22}$  neutrons/cm<sup>2</sup>. Recall from the discussion of PNL 5-31 that we do not consider the Westinghouse-PNL swelling equation<sup>18</sup> to be valid at fluences greater than this value. There is, however, a more recent<sup>28</sup> swelling equation for 20% cold-worked type 316 stainless steel:

$$\% \Delta V/V = A(\phi t)^{1.5} C(T)$$

where

$$A = 9 \times 10^{-35},$$

$$C(T) = 4.028 - 3.712 \times 10^{-2} T + 1.0145 \times 10^{-4} T^2 - 7.879 \times 10^{-8} T^3,$$

$$\phi t = \text{fast fluence, neutrons/cm}^2, \text{ and}$$

$$T = \text{temperature, } ^\circ\text{C}.$$

This equation is presently being used as the Fast Flux Test Facility (FFTF) design equation and is considered to be valid to  $2 \times 10^{23}$  neutrons/cm<sup>2</sup> fast fluence.<sup>29</sup> Notice that the equation given above has a fluence exponent of 1.5. The earlier equation<sup>18</sup> had a fluence exponent of 1.69 for 20% cold-worked type 316 stainless steel. Less swelling is predicted for the 1.5 power equation at all temperatures and fluences

than with the 1.69 power equation. The 1.5 power equation is considered to be representative of swelling in 20% cold-worked type 316 stainless steel in the absence of stresses. Stress-induced void formation may be significant above 500°C (refs. 28, 29) but we have not accounted for this phenomenon in our calculations for this pin. Even with this deficiency, we feel the predictions presented in Table 12 are more realistic than the predictions made using the 1.69 power cladding swelling equation, which predicted diametral expansions as high as 39 mils for this pin.

The summary page listed a total fluence of  $4.235 \times 10^{23}$  neutrons/cm<sup>2</sup> for this pin. Since no fast fluence value was given, we used the EBR-II conversion factor of 0.739, which was given in the data package. It has been recently suggested<sup>30</sup> that a factor of 0.55 is more appropriate.

#### MINT-2

The analysis of MINT-2 proved to be the most difficult of any problem in the round-robin exercise. The changes in power profile with burnup shown in Fig. IV.2 of Appendix A required major reprogramming of the FMØDEL code. In addition, operation of this pin as indicated in Fig. IV.1 of Appendix A for 8000 hr would result in more than 333 twenty-four-hour cycles. For analysis of this pin with the FMØDEL code, each 24-hr period is further divided into a rise to power (3 hr), a period of constant power operation (21.5 hr), and a period of low-power operation (0.5 hr). This results in approximately 1000 "FMØDEL cycles." Computer running time (using an IBM 360-91 computer) for an analysis using 36 FMØDEL cycles at the center axial node was about 5 min. Therefore, a detailed analysis considering all 1000 FMØDEL cycles would require nearly 2.5 hr of computer time for this axial node. We felt that such an expenditure of resources was not justified at this time and have, therefore, adopted a modified form of the irradiation history for use in this exercise.

During the 8000-hr operating history, about 1000 hr is spent rising to power, nearly 166 hr is spent at 0.1 relative power, and 480 hr is used in the initial rise to power. This leaves about 6350 hr of operation

at full power. We were interested in the influence of power cycling, especially the overpower cycles, at different burnups. Therefore we considered an irradiation history as shown in Fig. 3. Four time spans are shown on the x axis: 0 to 2048 hr, 2048 to 4096 hr, and so on. Each of these time spans is made up of nine FMØDEL cycles as shown. Cycle 8 in each time span represents steady-state operation at a peak heat rate of 16 kW/ft for approximately 2000 hr.

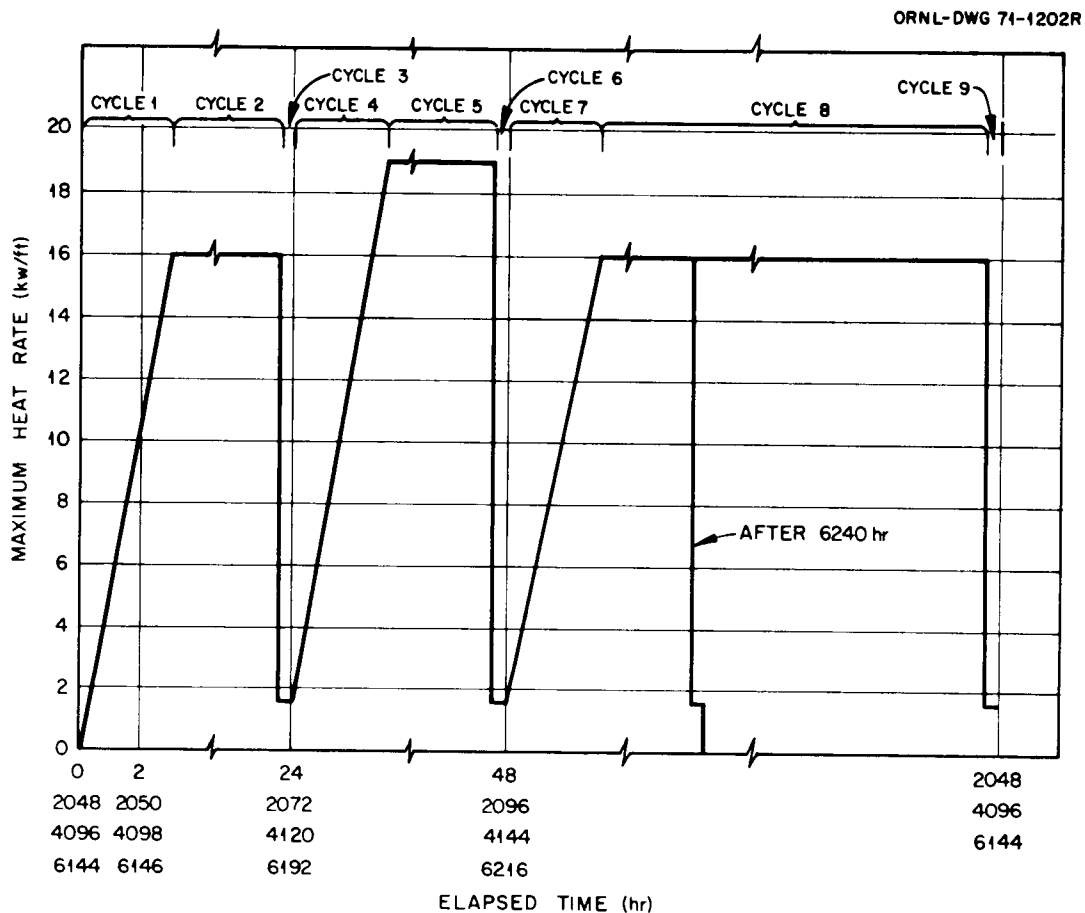


Fig. 3. Power Versus Time Relationship for MINT-2 (As Modeled).

Only three axial nodes were considered in this study. Due to the axial symmetry described in the data package for this pin, performance predictions for a position above the midplane of the pin will be identical to those for a like position below the midplane. A detailed tabulation of predicted performance parameters for axial positions 1, 3, and 5

(see Table 7, p. 9) at the end of the steady-state cycles of the simulated irradiation lifetime for this pin is presented in Table 17.

#### COMMENTS ON THE COMPARISON BETWEEN PREDICTED AND MEASURED PERFORMANCE

Postirradiation performance measurements were included in the data package for two pins in this study: F2Z and F2H. Comparisons between predicted performance and measured performance were presented in the previous section under the individual discussions of these pins. Agreement between prediction and measurement for F2Z was quite good. The predicted pin diametral expansions at all nine axial nodes fell between the measured 0 and 90° profilometer traces, and the predicted void and columnar grain region diameters were within 5% of the measured values. For F2H, the agreement was not as good. The predicted equiaxed and columnar grain region diameters were within about 6% of the measured values, but there was a 63% error in the predicted central void diameter. In addition, the predicted fuel pin diametral expansion values were consistently low in the central five axial regions.

We feel that the measured and predicted performance for F2H disagreed because the data provided in the data package did not accurately reflect the true operating conditions for this pin. For example, the data package lists the peak heat rate for this pin as 15.1 kW/ft. Other published sources list the peak heat rate as 16.5 to 17.2 kW/ft (ref. 31), 17.2 kW/ft (ref. 32), and 16.65 kW/ft at the beginning of life and 15.12 kW/ft at the end of life.<sup>33</sup> This last published heat rate information is the most recent and probably the most accurate. It seems obvious that the heat rate at the beginning of life was considerably higher than the 15.1 kW/ft peak heat rate given in the data package. Mechanical interaction between fuel and cladding was predicted due to differential thermal expansion on startup to 15.1 kW/ft peak heat rate. Therefore, a greater mechanical interaction would result if the initial peak heat rate were higher, resulting in additional plastic strain of the cladding and additional predicted diametral expansion of the pin.

Table 17. Performance Predictions for MINT-2 at End of Indicated Cycle

Cycle	Heat Rate (kW/ft)	Diametral Gap (mils)	Fuel Center Temperature (°C)	Fuel Cladding Contact Pressure (psi)	Void Diameter (in.)	Cladding Outer Hoop Stress (psi)	Fuel Burnup (% FIMA)	Cladding Outer Plastic Strain (%)	Cladding Hot ΔD/D (%)	Fuel Swelling (% ΔV/V)
<u>Axial Region 1</u>										
2	13.60	0	2312		0.0330	5476	0.037	3.46 × 10 <sup>-7</sup>	1.03	0.000815
5	16.16	0	2638		0.0355	6555	0.080	8.49 × 10 <sup>-7</sup>	1.04	0.0104
8	13.60	0.66	2058		0.0359	5942	2.22	2.88 × 10 <sup>-5</sup>	1.03	0.480
11	13.60	0.67	2085		0.0358	4943	2.25	2.91 × 10 <sup>-5</sup>	1.03	0.497
14	16.16	0	2619	101	0.0356	7028	2.29	2.97 × 10 <sup>-5</sup>	1.04	0.514
17	13.60	0.39	2190		0.0357	6568	4.42	6.22 × 10 <sup>-5</sup>	1.04	1.08
20	13.60	0.39	2190		0.0357	6566	4.45	6.25 × 10 <sup>-5</sup>	1.04	1.10
23	16.16	0	2627	202	0.0338	7657	4.50	6.32 × 10 <sup>-5</sup>	1.04	1.13
26	13.60	0	2206	462	0.0336	8207	6.63	1.13 × 10 <sup>-4</sup>	1.04	2.35
29	13.60	0	2207	427	0.0335	7982	6.66	1.14 × 10 <sup>-4</sup>	1.04	2.39
32	16.16	0	2676	427	0.0288	9067	6.71	1.15 × 10 <sup>-4</sup>	1.05	2.43
<u>Axial Region 3</u>										
2	15.01	0	2528		0.0364	5661	0.040	8.19 × 10 <sup>-7</sup>	1.13	0.00181
5	17.76	0	2800		0.0342	6684	0.0869	2.00 × 10 <sup>-6</sup>	1.14	0.0162
8	15.01	1.64	2466		0.0324	6114	2.43	6.97 × 10 <sup>-5</sup>	1.13	0.674
11	15.01	1.63	2466		0.0324	6124	2.46	7.04 × 10 <sup>-5</sup>	1.13	0.694
14	17.76	0.858	2800		0.0326	7148	2.49	7.14 × 10 <sup>-5</sup>	1.14	0.713
17	15.01	1.16	2450		0.0329	6751	4.83	1.54 × 10 <sup>-4</sup>	1.14	1.47
20	15.01	1.15	2450		0.0329	6743	4.86	1.54 × 10 <sup>-4</sup>	1.14	1.50
23	17.76	0.362	2800		0.0330	7769	4.90	1.56 × 10 <sup>-4</sup>	1.14	1.54
26	15.01	0.268	2447		0.0332	7385	7.23	2.56 × 10 <sup>-4</sup>	1.14	2.88
29	15.01	0.250	2447		0.0332	7360	7.26	2.57 × 10 <sup>-4</sup>	1.14	2.92
32	17.76	0	2800	416	0.0296	9119	7.31	2.59 × 10 <sup>-4</sup>	1.15	2.96
<u>Axial Region 5</u>										
2	16.00	0	2690		0.0375	5483	0.043	3.48 × 10 <sup>-6</sup>	1.20	0.00375
5	19.00	0	2800		0.0401	6551	0.0923	8.57 × 10 <sup>-6</sup>	1.21	0.0219
8	16.00	0.409	2555		0.0406	5867	2.58	2.96 × 10 <sup>-4</sup>	1.20	0.807
11	16.00	0.409	2555		0.0406	5923	2.61	3.00 × 10 <sup>-4</sup>	1.20	0.829
14	19.00	0	2800		0.0383	6998	2.66	3.06 × 10 <sup>-4</sup>	1.21	0.854
17	16.00	0.244	2567		0.0385	6539	5.14	6.66 × 10 <sup>-4</sup>	1.21	1.81
20	16.00	0.228	2567		0.0385	6516	5.17	6.69 × 10 <sup>-4</sup>	1.21	1.85
23	19.00	0	2800	315	0.0349	8317	5.22	6.78 × 10 <sup>-4</sup>	1.22	1.89
26	16.00	0	2604	457	0.0349	8258	7.70	1.30 × 10 <sup>-3</sup>	1.21	3.28
29	16.00	0	2606	417	0.0347	7817	7.74	1.31 × 10 <sup>-3</sup>	1.21	3.33
32	19.00	0	2800	417	0.0287	8897	7.79	1.32 × 10 <sup>-3</sup>	1.22	3.36

In addition to this, the peak total neutron fluence given for this pin in the data package is  $5.55 \times 10^{22}$  neutrons/cm<sup>2</sup>. A conversion factor of 0.739 is suggested in the data package for converting total fluences to fast fluences for use with the Westinghouse-PNL swelling equations. However, the peak total and fast fluences reported in the literature<sup>34</sup> for subassembly XG05 (in which F2H was irradiated) are 5.69 and  $5.011 \times 10^{22}$  neutrons/cm<sup>2</sup>, respectively. These data suggest a conversion factor of 0.881 for converting total fluences to fast fluences for this pin. If this conversion factor had been applied to the F2H calculations presented in this study the cladding swelling would have been based on a peak fast fluence of  $4.89 \times 10^{22}$  neutrons/cm<sup>2</sup> instead of  $4.10 \times 10^{22}$  neutrons/cm<sup>2</sup>. This would also have increased the predicted diametral expansion of the pin.

These comments explain the low predicted diametral expansions of the pin, but do not explain the large error in the predicted central void diameter.

#### SUMMARY

The FMØDEL computer code was used to predict the irradiation performance of eight fuel pins in a round-robin exercise. A number of assumptions are built into this code that influence the results of such a study. These assumptions were stated and justified with regard to the problems in the exercise. The data package used for this exercise was included in this document as an appendix, and the conversion of information from this package to input data for the FMØDEL code was tabulated. Performance predictions were tabulated and commented upon.

The performance predictions for F2H and F2Z (the only pins in the exercise for which postirradiation data were included in the data package) are in reasonable agreement with postirradiation measurements, which lends support to the validity of our assumptions.

No attempt was made to apply a cladding damage or failure criterion to the eight pins in this exercise.

## REFERENCES

1. C. M. Cox and F. J. Homan, "Analysis of a Mixed-Oxide Fuel Pin Performance Using the FMODEL Computer Code," (Summary) Trans. Am. Nucl. Soc. 12(2), 536 (1969).
2. C. M. Cox and F. J. Homan, "Performance Analysis of a Mixed Oxide LMFBR Fuel Pin," Nucl. Appl. Technol. 9(3), 317-325 (1970).
3. F. J. Homan, "Fuel-Cladding Mechanical Interaction During Startup," (Summary) Trans. Am. Nucl. Soc. 13(2), 576 (1970).
4. W. E. Baily, E. A. Aitken, R. R. Asamoto, and C. N. Craig, "Thermal Conductivity of Uranium-Plutonium Oxide Fuels," pp. 293-308 in International Symposium on Plutonium Fuels Technology, Scottsdale, Arizona, 1967, Nucl. Met. 13, American Institute of Mining, Metallurgical and Petroleum Engineers, New York, 1968.
5. A. Wolfe and S. F. Kaufman, Mechanical Properties of Oxide Fuels, WAPD-TM-587, pp. 118-119 (October 1967).
6. Ibid., pp. 3-26.
7. R. E. Adams, private communication, September 1968.
8. P. E. Bohaboy, R. R. Asamoto, and A. E. Conti, Compressive Creep Characteristics of Stoichiometric Uranium Dioxide, GEAP-10054 (May 1969).
9. A. H. Clauer et al., Progress Report on Development of Materials and Technology for Advanced Reactors, BMI-1862, p. C-22 (January-March 1969).
10. C. M. Cox, LMFBR Fuel Cycle Studies Progress Report for March 1970, No. 13, ORNL-TM-2949, p. 85.
11. F. J. Homan, LMFBR Fuel Cycle Studies Progress Report for January 1971, No. 23, ORNL-TM-3312.
12. G. W. Greenwood and M. V. Speight, J. Nucl. Mater. 10(2), 140-144 (1963).
13. I. Goldberg, L. L. Lynn, and C. D. Sphar, FIGRO-FORTRAN IV Digital Computer Program for the Analysis of Fuel Swelling and Calculation of Temperature in Bulk Oxide Cylindrical Fuel Elements, WAPD-TM-618 (December 1966).
14. U.S. Steel (National Tube Division), Bulletin No. 26, 59th Edition, p. 62.
15. F. J. Homan, Fuels and Materials Development Program Quart. Progr. Rept. June 30, 1970, ORNL-4600, p. 74.

16. Metals Handbook, Vol. 1, Properties and Selection of Metals, 8th Edition, 1961, p. 423.
17. A. Biancheria et al., Oxide Fuel Element Development Quart. Progr. Rept. Sept. 30, 1969, WARD-4135-1, p. 19.
18. Ibid., p. 6.
19. T. T. Claudson, Irradiation Induced Swelling and Creep in Fast Reactor Materials, BNWL-SA-3283, 21 May 1970.
20. C. M. Cox, R. B. Fitts, and F. J. Homan, Fuels and Materials Development Program Quart. Progr. Rept. March 31, 1969, ORNL-4420, pp. 33-37.
21. R. B. Fitts, E. L. Long, Jr., and D. R. Cuneo, LMFBR Fuel Cycle Studies Progress Report for November 1970, No. 21, ORNL-TM-3250, pp. 71-74.
22. P. E. Bohaboy, "Creep Properties of Mixed Plutonium-Uranium Oxides," paper presented at the 72nd Annual Meeting of the American Ceramic Society, May 2-7, 1970, Philadelphia, Pennsylvania.
23. J. S. Perrin, R. A. Robinson, and S. J. Basham, "Enhancement of Creep in Uranium Dioxide During Irradiation," paper presented at the 72nd Annual Meeting of the American Ceramic Society, May 2-7, 1970, Philadelphia, Pennsylvania.
24. R. C. Nelson et al., Performance of Plutonium-Uranium Mixed-Oxide Fuel Pins Irradiated in a Fast Reactor (EBR-II) to 50,000 Mwd/Te, GEAP-13549, pp. 93-94 (August 1969).
25. R. C. Nelson et al., op. cit., Appendix B.
26. W. E. Baily, Sodium-Cooled Reactors, Fast Ceramic Reactor Development Program, 30th Quart. Rept. February-April 1969, GEAP-10028, pp. 6-10.
27. F. J. Homan, LMFBR Fuel Cycle Studies Progress Report for December 1970, ORNL-TM-3281, pp. 62-68.
28. Private communication from Peter Murray, WARD, to P. G. Shewmon, ANL, January 26, 1971.
29. Private communication from A. Biancheria, WARD, to F. J. Homan, ORNL, February 1971.
30. Private communication from G. A. Last, WADCO, to L. Bernath, A. Boltax et al., February 12, 1971.
31. W. E. Baily and E. L. Zebroski, GEAP-10028, op. cit., pp. 6-26.

32. R. E. Skavdahl and E. L. Zebroski, Sodium-Cooled Reactors Fast Ceramic Reactor Development Program, Twenty-Seventh Quarterly Report May-July 1968, GEAP-5677, p. 60.
33. W. E. Baily and E. L. Zebroski, Sodium-Cooled Reactors Fast Ceramic Reactor Development Program, Thirty-Fourth Quarterly Report February-April 1970, GEAP-10028-34, p. 48.
34. W. E. Baily and E. L. Zebroski, Sodium-Cooled Reactors Fast Ceramic Reactor Development Program, Thirty-Fifth Quarterly Report, May-July 1970, GEAP-10028-35, pp. 11-12.

APPENDIX A



DATA SUPPLIED THE WORKING GROUP FOR THE  
EIGHT-PIN ROUND-ROBIN EXERCISE

The data for this exercise were supplied by the sites responsible for irradiation of the individual pins and were compiled by D. C. Bullington. The data package was forwarded to the working group members with Bullington's letter of September 15, 1970 (hereinafter referred to as Bullington's letter) to L. Bernath et al. Some additional data and several copies of a suggested format for reporting results were forwarded later with R. D. Leggett's letter of October 15, 1970 (hereinafter referred to as Leggett's letter) to L. Bernath et al. Tables A1 and A2 are the summaries of problem parameters included with Bullington's and Leggett's letters, respectively.

A considerable amount of detailed data was included with Bullington's letter. These data are included here as Annex I (Reference Standard-F2H and F2Z), Annex II [Irradiation Test Conditions-Elements PNL 3-30 (X-054) and PNL 5-31 (X-051)], Annex III (LMFBR Demonstration Plant), and Annex IV (ORNL Power Cycle Test). Annex I and Annex II have appendices of their own (Appendix I and Appendix II, respectively) which should not be confused with Appendix A of this document.

Postirradiation profilometry traces for F2H and F2Z were included with Bullington's letter. These traces are not included here because they are incorporated into the body of this work. Preirradiation cladding profilometry traces for PNL 3-30 and 5-31 were included with Leggett's letter. These traces are not included here because preirradiation cladding diameters for these pins are given in Annex II.

Table A1. Summary of Problem Parameters

Parameter	F2H	F2Z	PNL 3-30	PNL 5-31	PNL 3-30 Modified	Demo Plant	Demo CW Cladding	ORNL MINT
Initial peak linear power, kW/ft	15.1	14.2	5.58	14.7	14.7	15.0	15.0	16.0 <sup>a</sup>
Cladding	Type 316 stainless steel, annealed	Type 316 stainless steel, annealed	Type 304 stainless steel, annealed	Type 304 stainless steel, annealed	Type 304 stainless steel, annealed	Type 316 stainless steel, 20% cold worked	Type 316 stainless steel, 20% cold worked	Type 316 stainless steel, 20% cold worked
Peak cladding temperature, °F	963	947	794	924	794	1094	1094	1000 at 16 kW/ft
Neutron flux at startup, neutrons cm <sup>-2</sup> sec <sup>-1</sup> (> 0.1 MeV)	2.07 × 10 <sup>15</sup>	2.07 × 10 <sup>15</sup>	1.95 × 10 <sup>15</sup> 1.71 × 10 <sup>15</sup>	1.72 × 10 <sup>15</sup> 1.47 × 10 <sup>15</sup>	To be specified			1.26 × 10 <sup>13</sup>
Fuence, neutrons/cm <sup>2</sup> (> 0.1 MeV)	5.55 × 10 <sup>22</sup>	4.18 × 10 <sup>22</sup>	5.15 × 10 <sup>22</sup> 4.52 × 10 <sup>22</sup>	3.31 × 10 <sup>22</sup> 2.88 × 10 <sup>22</sup>	To be specified	4.135 × 10 <sup>22</sup>	4.135 × 10 <sup>22</sup>	
Fuel density, % of theoretical								
Pellet	96.1	89.2	90.5	91.5	90.5	83.76	89.00	92.0
Smearred	94.0	86.5	86.6	86.5	86.6	80.0	85.00	90.1
Burnup, Mwd/metric ton	59,727	41,465	27,270	53,600	53,600	100,000	100,000	72,500

<sup>a</sup>19.0 overpower.

Table A2. Summary of Problem Parameters

Parameter	F2H	F2Z	PNL 3-30	PNL 5-31	PNL 5-31 Modified	Demo Plant		ORNL MINT
						80% Dense	85% Dense	
Initial peak linear power, kW/ft	15.1	14.2	5.58	14.7	14.7	15.0	15.0	16.0 <sup>a</sup>
Cladding	Type 316 stainless steel, annealed	Type 316 stainless steel, annealed	Type 304 stainless steel, annealed	Type 304 stainless steel, annealed	Type 304 stainless steel, annealed	Type 316 stainless steel, 20% cold worked	Type 316 stainless steel, 20% cold worked	Type 316 stainless steel, 20% cold worked
Peak cladding temperature, °F	963	947	794	924	924	1094	1094	1000 at 16 kw/ft
Neutron flux at startup, neutrons cm <sup>-2</sup> sec <sup>-1</sup> (> 0.1 MeV)	2.07 × 10 <sup>15</sup>	2.07 × 10 <sup>15</sup>	1.95 × 10 <sup>15</sup> 1.71 × 10 <sup>15</sup>	1.72 × 10 <sup>15</sup> 1.47 × 10 <sup>15</sup>	7 × 10 <sup>15</sup> 4.55 × 10 <sup>15</sup>			1.26 × 10 <sup>13</sup>
Fluence, neutrons/cm <sup>2</sup> (> 0.1 MeV)	5.55 × 10 <sup>22</sup>	4.18 × 10 <sup>22</sup>	5.15 × 10 <sup>22</sup> 4.52 × 10 <sup>22</sup>	3.31 × 10 <sup>22</sup> 2.88 × 10 <sup>22</sup>	1.35 × 10 <sup>23</sup> 8.75 × 10 <sup>22</sup>	4.135 × 10 <sup>23</sup>	4.135 × 10 <sup>23</sup>	
Fuel density, % of theoretical								
Pellet	96.1	89.2	90.5	91.5	91.5	83.76	89.00	92.0
Smeared	94.0	86.5	86.6	86.5	86.5	80.0	85.0	90.1
Burnup, MWd/metric ton	59,727	41,465	27,270	53,600	53,600	100,000	100,000	72,500

<sup>a</sup>19.0 overpower.

## Annex I

I. Reference Standard - F2H and F2Z

The following pre- and postirradiation data were supplied by GE-BRDO and EBR-II for irradiation experiments F2H and F2Z. Since both the preirradiation parameters, detailed irradiation conditions, and postirradiation observations are supplied, the data can be used to calibrate models to predict the behavior of pins supplied in later sections.

A. Irradiation Test Conditions

The information on irradiation test conditions consists of two parts, a time-power history, which is on punched cards, and a description of the environment at 45 MW(t). Figures I.1(a) and I.1(b) give the power generation profiles and the total flux profile in the fueled regions of elements F2H and F2Z at 45 MW(t). Figures I.2 and I.3 give the external sodium temperature and the temperature profiles of the outside surface of the cladding at 45 MW(t). The following is a discussion of the basis for the information presented in Figs. I.1, I.2, and I.3.

Power Generation Profiles

Both of these elements were loaded into EBR-II at the start of run 8 (September 1965). Since that time there have been a number of changes in the EBR-II core, some of which occurred while these elements were in test. As a result of these changes, the fission rates given in the current revision of the Guide for Irradiation Experiments in EBR-II cannot be used directly to calculate the power generation profiles in these two elements. To obtain the curves given in Fig. I.1 the mid-plane fission rates were calculated as follows.

Element - F2Z: Loaded at start of run 8.  
Removed at end of run 24.  
Position - 4E2.  
Total exposure - 9318 Mwd/metric ton.

From Table V, Revision 2, Guide for Irradiation Experiments in EBR-II:

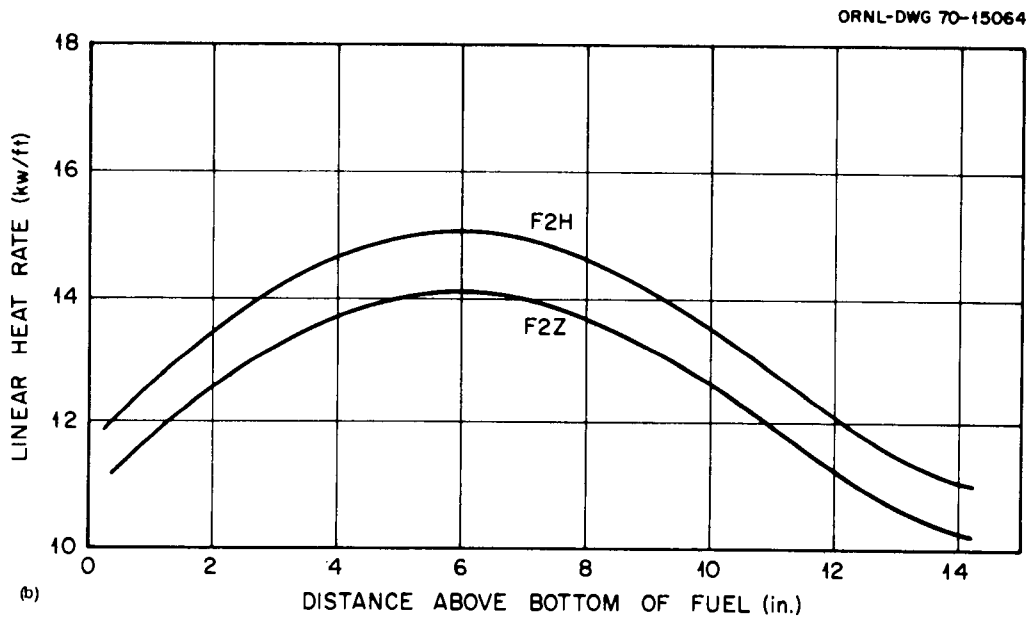
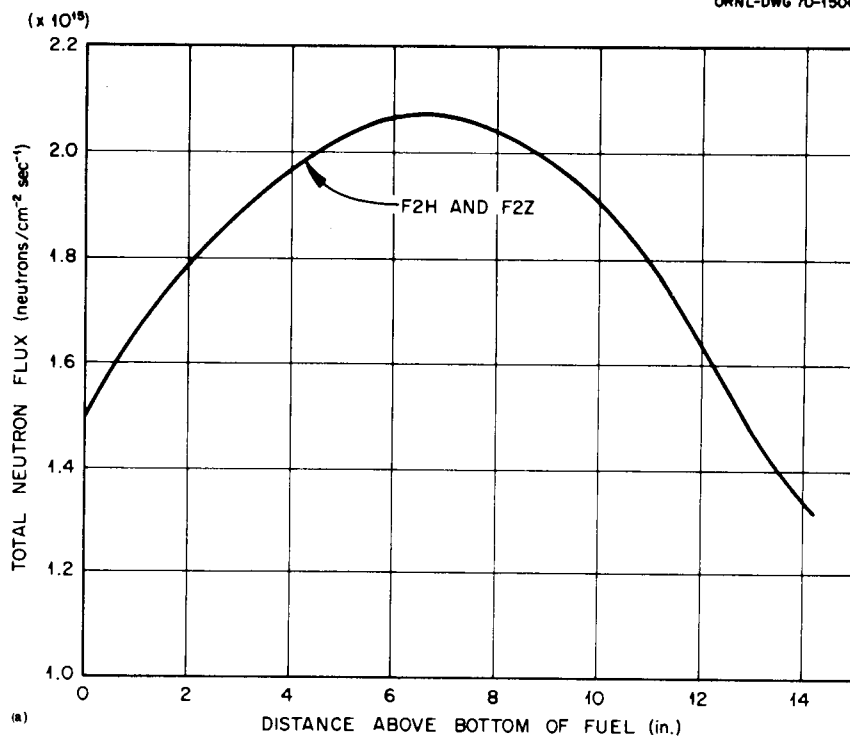


Fig. I.1. Flux Profiles for F2H and F2Z at 45 MW(t). (a) Total neutron flux and (b) linear heat rate.

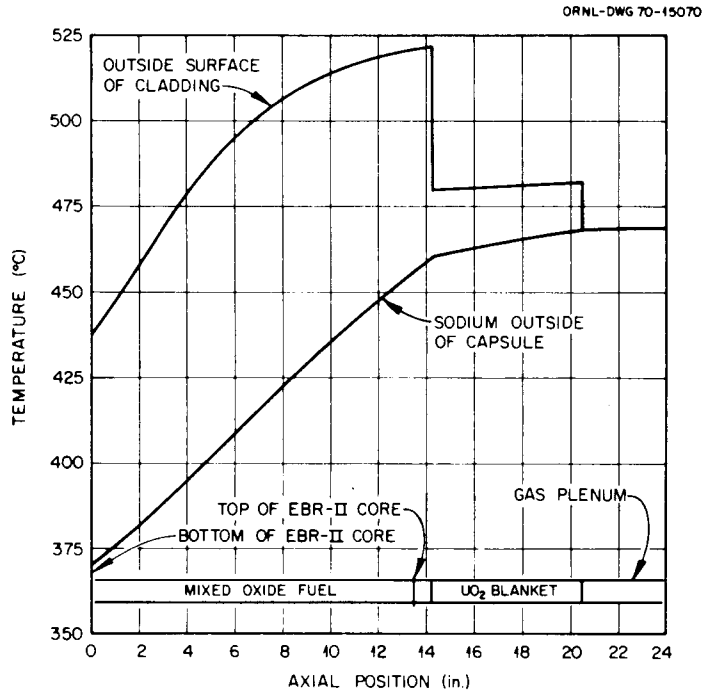


Fig. I.2. Element F2H Cladding Temperature Profile at 45 MW(t).

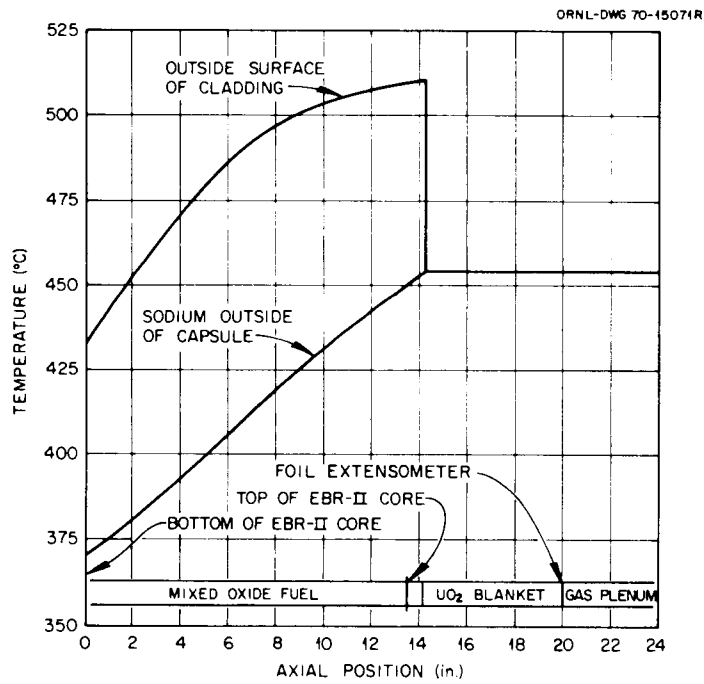


Fig. I.3. Element F2Z Cladding Temperature Profile at 45 MW(t).

$^{235}\text{U}$  fission rate =  $1.105 \times 10^{13}$  fissions  $\text{g}^{-1} \text{sec}^{-1}$  at 62.5 MW(t)  
 $^{238}\text{U}$  fission rate =  $0.725 \times 10^{12}$  fissions  $\text{g}^{-1} \text{sec}^{-1}$  at 62.5 MW(t)  
 $^{239}\text{Pu}$  and  $^{240}\text{Pu}$  fission rate =  $1.336 \times 10^{13}$  fissions  $\text{g}^{-1} \text{sec}^{-1}$  at  
 62.5 MW(t)

The fuel loading was obtained from the as-fabricated data given in Table I of the Hazards Evaluation by W. W. Kendall, 2/23/65.

Total weight of mixed oxide - 84.62 g

$^{235}\text{U}$  = 93.0%

Total Pu = 20 ± 1%.

The measured peak burnup was 4.68 at. % (see pp. 7-21 of GEAP-10028-32).

The fission rates were corrected to 45 MW(t) and were reduced by 5%. This 5% reduction was made to account for an observed difference between the measured and calculated burnup of driver fuel. The fuel loading was reduced by 2% to account for depletion. This represents the average fuel loading over the life of the test. Using the above information, the peak linear heat rate was calculated to be 14.1 kW/ft. The axial heat generation profile was obtained by assuming that the local heat generation rate was proportional to the relative  $^{235}\text{U}$  fission rate as given in Fig. C-1 of the current revision of the Guide for Irradiation Experiments in EBR-II. As an overall check, the peak burnup was calculated using the history-averaged core midplane fission rate described above. The calculated burnup was 5.11 at. % as compared to a measured burnup of 4.68 at. %.

Element - F2H: Loaded at start of run 8.  
 Removed at end of run 27B.  
 Out of reactor for run 27A.  
 Position - 4C2.  
 Total exposure - 12,641 MWd/metric ton.

The overall procedure followed for F2H was the same as for F2Z. However, since it was in the reactor when the stainless steel reflector was installed, the history-averaged core midplane fission rate was adjusted for this perturbation. The fuel loading was reduced 3% to correct for depletion, and the fission rate was reduced by 5% as discussed for F2Z. The resulting peak linear heat rate was 15.05 kW/ft. The

---

\*Suspect  $^{241}\text{Pu}$ .

corresponding peak burnup was calculated to be 6.81 at. % compared to a measured value of 6.75 at. %.

#### Total Flux Profile

The total flux profile given in Fig. I.1 applies to both elements at 45 MW(t). It was obtained from Fig. C-3 of the Guide for Irradiation Experiments in EBR-II with the peak flux normalized on the basis of the history-averaged fission rates described in the previous section. Since this flux profile contains the 5% reduction factor, the appropriate correction factor for use of the PNL-Westinghouse stainless steel swelling correlation is  $(0.85/1.15 = 0.739)$  rather than  $(0.85/1.2 = 0.708)$ .

#### Temperature Profiles

Figures I.2 and I.3 present the temperature profiles of the outside surface of the cladding at 45 MW(t). The sodium temperature outside the capsule is shown for reference. The capsule heat transfer calculations were done with a code written by G. Golden which has been incorporated into the LIFE code. The additional temperature rise in the sodium beyond the end of the fuel region in F2H is due to the axial blanket which contains 25%  $^{235}\text{U}$ . Element F2Z has a natural uranium blanket and hence does not show significant heat generation in this region. The estimation of the fission rate in the blanket region of element F2H was quite crude and is susceptible to large errors. However, since the total rise in the sodium temperature in the blanket region is only  $14^\circ\text{F}$ , the effect of this uncertainty on the temperature of the cladding in the plenum region is small.

#### History

F2Z was loaded into EBR-II starting with run 8 on September 7, 1965, and was in the reactor 480.7 days through run 24 on December 31, 1966. The equivalent number of full power days obtained by dividing the total megawatt days by 45 MW(t) gives  $9318/45 = 207.1$  equivalent days at full power.

Figure I.4 presents a detailed history of the run 8 approach to power. This startup for both F2H and F2Z is included for those who

ORNL-DWG 71-1369

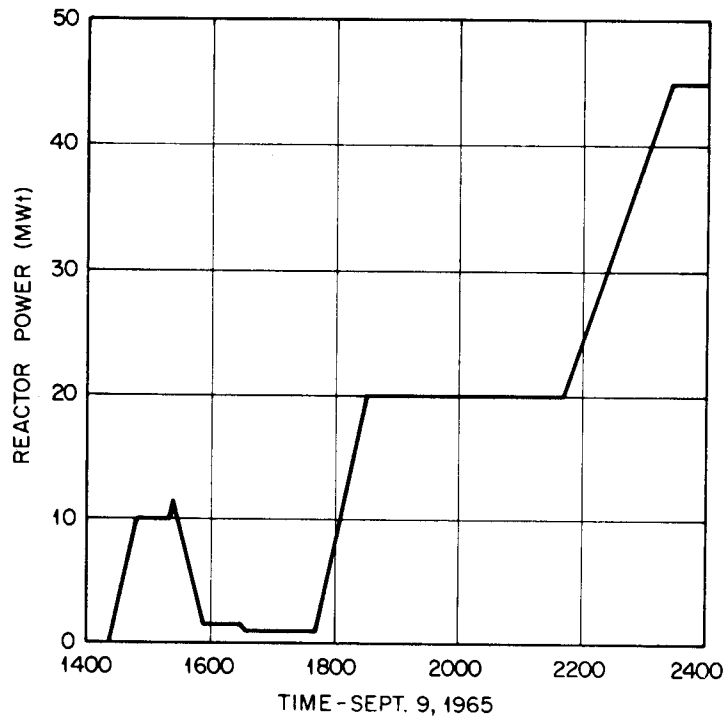


Fig. I.4. Approach to Power - EBR-II Run 8.

wish to consider thermal expansion induced mechanical interaction on the first startup in detail.

F2H also loaded into EBR-II at the start of run 8 was in the reactor a total of 911 days. It was discharged at the end of run 27B on March 5, 1968. During its irradiation history it was removed from the core during run 27A (2/2/68-2/29/68).

The deck of Fortran cards sent under separate cover indicate the EBR-II power history for runs 8 through 27B with the exception of 27A. The two data fields which appear on the cards (Fortran format E15.6, E15.4) indicate the elapsed time in days and the reactor power in MW(t). When the reactor is down, 0.001 MW(t) is specified rather than zero. The cards provide a linear fit of the EBR-II operating history as described in the EBR-II Experimental Program Operating Summaries for the time period covered. All of the cards are needed for the history of F2H. Only cards up to and including day 480.7 are needed for the F2Z history.

For models that require less precise power histories the deck was analyzed to determine the total time F2H was at full power [reactor was at 45 MW(t)]. The equivalent days at full power obtained by dividing the accumulated megawatt days by 45 MW(t) gives  $12,641/45 = 280.9$  equivalent days. Examination of the deck, however, indicates F2H was at full power only 214.1 days. It reached full power 155 times. It was also over power 17.8 min at 605.8 days into the run when the reactor went to 50 MW(t).

The number of times the power was reduced from 45 MW(t) was also determined. During the 911 days F2H was in EBR-II, the reactor lost over 10% of power 159 times. The percent loss in power from 45 MW(t) and the number of reactor cycles are shown below. Only loss of power following full power operation is included.

<u>Percent Loss of Reactor Power After Reaching 45 MW(t)</u>	<u>Total Number of Cycles Which Exceed the Percentage Indicated</u>
10	159
20	152
40	123
60	114
80	109
100	105

B. Burnup and Fluence Summary

<u>Capsule Identification</u>	<u>F2H</u>	<u>F2Z</u>
Calculated peak burnup, MWd/metric ton*	65,287	49,141
Peak burnup from Nd-148, MWd/metric ton*	60,354	42,804
Peak burnup from heavy element analysis, MWd/metric ton*	59,727	41,465
Calculated peak total fluence, neutrons/cm <sup>2</sup>	$5.55 \times 10^{22}$	$4.18 \times 10^{22}$

---

\*Assumes 192 MeV/fission.

C. Preirradiation Fuel Parameters

<u>Capsule Identification</u>	<u>F2H</u>	<u>F2Z</u>
Fuel type	Solid pellet	Solid pellet
Form	Coprecipitated	Coprecipitated
PuO <sub>2</sub> , %	19.6-20.5	20.0
Density, % of theoretical		
Pellet	93.0-97.1	88.2-90.2
Mean	96.1	89.2
Stoichiometry, O/M	1.974-1.986	1.983-1.999
Mean O/M	1.978	1.988
Weight, g	92.084	84.63
Length, in.*	14.266	14.210
Mean pellet diameter, in.	0.2177	0.2171
Fuel-cladding diametral gap, mils†	1.2-5.0	2.1-4.8

D. Preirradiation Cladding Parameters

<u>Capsule Identification</u>	<u>F2H</u>	<u>F2Z</u>
Cladding, type stainless steel	316	316
Condition	Annealed	Annealed
Diameter, in.		
Inside	0.2203-0.2205	0.2201-0.2208
Outside‡	0.2484-0.2495	0.2485-0.2490
Mean outside diameter, in.	0.2491	0.2488
Nominal wall, mils	15	15

---

\* Total length measured before loading.

† The local diametral gap can be determined from the pellet diameters in Appendix I.

‡ For cladding outside diameter as a function of length, see Table I.3, Appendix I.

E. Postirradiation Data

Transverse metallographic section observations:

Capsule Identification	F2H	F2Z
Distance from bottom of fuel to section, in.	11.86	6.521
Local linear power of specimen/axial peak linear power of fuel pin*	0.7794	0.9951
Fuel-cladding gap, mils		
Preirradiation	4.8	4.1
Postirradiation	0	0
Preirradiation pellet diameter, in.	0.2155	0.2162
Void diameter, in.†	0.0109±0.0002	0.0465±0.0004
Equiaxed grain growth diameter, in. †	0.1605±0.0025	not distinguishable
Columnar grain growth diameter, in. †	0.1027±0.0045	0.1434±0.0035
Preirradiation cladding outside diameter‡	0.2491	0.2490
Postirradiation cladding outside diameter obtained at 11.86 in. from bottom of fuel column§	0.25068	0.24932
Length change of fuel column	No length change observed to ± 1/32 in.	
Calculated fission gas formed, cm <sup>3</sup> **	122.4	84.2
Fission gas released, cm <sup>3</sup>	91.8	54.3
Fission gas release, %	75.0	64.5

\* Determined from gamma scan.

† 90% confidence based upon nine observations.

‡ Interpolation from Table I.3 in Appendix I.

§ See profilometer data in Appendix I.

\*\* Assumes 24.6 fission gas atoms for every 100 fissions.

APPENDIX I



Table I.1. Miscellaneous Preirradiation Information

Capsule Identification	F2H	F2Z
Capsule type, stainless steel	304	304
Nominal capsule diameter, in.		
Outside	0.375	0.375
Inside	0.335	0.335
Approximate fuel pin plenum volume, cm <sup>3</sup>	8.11	8.11

Table I. 2. Fuel Isotopics

Powder Source	Content, <sup>235</sup> U, %		Plutonium Content, at. %			
	PuO <sub>2</sub>	Total U	<sup>239</sup> Pu	<sup>240</sup> Pu	<sup>241</sup> Pu	<sup>242</sup> Pu
			<u>F2H</u>			
B-25	20.3	93.3	91.56	7.74	0.702	
B-26	19.9	94.0	90.99	8.20	0.772	0.03
B-48	20.0	93.7	90.96	8.22	0.764	0.04
B-49	20.5	93.0	90.92	8.27	0.770	0.03
B-53	19.7	91.58	91.03	8.17	0.761	0.03
B-65	19.9	93.8	91.04	8.16	0.765	0.03
B-66	19.6	91.7	90.90	8.29	0.769	0.03
			<u>F2Z</u>			
B-95	20.0	93.0	90.98	8.27	0.715	0.04
B-96	20.6	91.0	90.90	8.31	0.71	0.03

Table I.3. Outside Diameter of Cladding Before Irradiation

Distance from Bottom of Pin <sup>a</sup> (in.)	F2H		F2Z	
	0-180°	90-270°	0-180°	90-270°
1	0.2493	0.2484	0.2485	0.2485
2	0.2490	0.2488	0.2485	0.2485
3	0.2491	0.2490	0.2485	0.2485
4	0.2492	0.2492	0.2485	0.2490
5	0.2495	0.2490	0.2485	0.2485
6	0.2493	0.2490	0.2490	0.2485
7	0.2492	0.2491	0.2490	0.2490
8	0.2491	0.2491	0.2485	0.2490
9	0.2491	0.2492	0.2485	0.2485
10	0.2492	0.2492	0.2485	0.2485
11	0.2490	0.2490	0.2490	0.2485
12	0.2493	0.2493	0.2490	0.2490
13	0.2491	0.2490	0.2490	0.2490
14	0.2490	0.2490	0.2490	0.2490
15	0.2490	0.2490	0.2490	0.2490
16	0.2490	0.2488	0.2490	0.2490
17	0.2490	0.2490	0.2490	0.2490
18	0.2490	0.2490	0.2490	0.2490
19	0.2490	0.2487	0.2490	0.2490

<sup>a</sup>Bottom of fuel column is 0.89 in. above bottom of pin.

Table I.4. F2H Pellet Fabrication Data

Pellet Number	Distance from Bottom of Fuel to Top of Pellet (in.)	Pellet		Ratio O: Metal	Batch Number
		Diameter (in.)	Density (g/cm <sup>3</sup> )		
1	0.2501	0.2181	10.2590	1.974	B-26
2	0.5009	0.2172	10.6110	1.976	B-53
3	0.7526	0.2179	10.4402	1.976	B-53
4	0.9938	0.2181	10.6376	1.974	B-25
5	1.2353	0.2190	10.5372	1.974	B-25
6	1.5083	0.2185	10.5271	1.979	B-66
7	1.7793	0.2173	10.5096	1.979	B-65
8	2.0506	0.2184	10.4106	1.979	B-65
9	2.3216	0.2175	10.5510	1.979	B-65
10	2.5916	0.2179	10.5633	1.979	B-65
11	2.8594	0.2186	10.5395	1.979	B-65
12	3.1314	0.2180	10.4640	1.979	B-65
13	3.4024	0.2186	10.4451	1.979	B-65
14	3.6704	0.2188	10.5427	1.979	B-65
15	3.9389	0.2191	10.5003	1.979	B-65
16	4.2073	0.2188	10.5270	1.979	B-65
17	4.4753	0.2190	10.5234	1.979	B-65
18	4.7435	0.2188	10.5348	1.979	B-65
19	5.0099	0.2187	10.5974	1.979	B-65
20	5.2787	0.2178	10.5958	1.979	B-65
21	5.5472	0.2175	10.6186	1.979	B-65
22	5.8168	0.2171	10.6143	1.979	B-65
23	6.0843	0.2177	10.6081	1.979	B-65
24	6.3530	0.2180	10.5925	1.979	B-65
25	6.6196	0.2187	10.5955	1.979	B-65
26	6.8882	0.2187	10.5166	1.979	B-65
27	7.1594	0.2168	10.6114	1.979	B-65
28	7.4349	0.2174	10.5076	1.976	B-66
29	7.7102	0.2182	10.2010	1.978	B-66
30	7.9860	0.2177	10.5267	1.978	B-66
31	8.2642	0.2176	10.4455	1.978	B-66
32	8.5427	0.2170	10.4920	1.978	B-66
33	8.8207	0.2171	10.5012	1.978	B-66
34	9.0973	0.2168	10.5836	1.978	B-66
35	9.3748	0.2169	10.5395	1.978	B-66
36	9.6483	0.2179	10.4760	1.983	B-66
37	9.9092	0.2187	10.4346	1.986	B-66
38	10.1838	0.2168	10.5402	1.986	B-66
39	10.4638	0.2160	10.5327	1.976	B-53
40	10.7386	0.2180	10.5360	1.976	B-53
41	11.0163	0.2169	10.5617	1.976	B-53
42	11.2915	0.2179	10.5898	1.976	B-53

Table I.4 (continued)

Pellet Number	Distance from Bottom of Fuel to Top of Pellet (in.)	Pellet		Ratio O: Metal	Batch Number
		Diameter (in.)	Density (g/cm <sup>3</sup> )		
43	11.5662	0.2187	10.5789	1.978	B-49
44	11.8409	0.2186	10.6005	1.978	B-49
45	12.1222	0.2155	10.6220	1.976	B-53
46	12.4004	0.2162	10.6410	1.976	B-53
47	12.6799	0.2165	10.5918	1.976	B-53
48	12.9550	0.2175	10.6327	1.976	B-53
49	13.2320	0.2169	10.6182	1.977	B-49
50	13.5090	0.2165	10.6336	1.977	B-49
51	13.7870	0.2164	10.6290	1.977	B-49
52	14.0644	0.2164	10.6520	1.977	B-49
53	14.3290	0.2185	10.4798	1.977	B-49

Table I.5. F2Z Pellet Fabrication Data

Pellet Number	Distance from Bottom of Fuel to Top of Pellet (in.)	Pellet		Ratio O: Metal	Batch Number
		Diameter (in.)	Density (g/cm <sup>3</sup> )		
1	0.2734	0.2175	9.7311	1.989	B-96
2	0.5491	0.2175	9.6797	1.983	B-96
3	0.8236	0.2171	9.7158	1.983	B-96
4	1.0982	0.2169	9.7663	1.983	B-96
5	1.3721	0.2165	9.8456	1.983	B-96
6	1.6458	0.2168	9.7833	1.983	B-96
7	1.9200	0.2168	9.7896	1.983	B-96
8	2.1926	0.2177	9.7176	1.999	B-95
9	2.4644	0.2178	9.7674	1.999	B-95
10	2.7365	0.2179	9.7417	1.999	B-95
11	3.0095	0.2167	9.8538	1.989	B-96
12	3.2824	0.2167	9.8453	1.989	B-96
13	3.5558	0.2166	9.8424	1.989	B-96
14	3.8280	0.2167	9.8828	1.989	B-96
15	4.1019	0.2169	9.8214	1.989	B-96
16	4.3758	0.2170	9.7883	1.989	B-96
17	4.6546	0.2177	9.8192	1.992	B-95
18	4.9346	0.2180	9.7912	1.992	B-95

Table I.5 (continued)

Pellet Number	Distance from Bottom of Fuel to Top of Pellet (in.)	Pellet		Ratio O: Metal	Batch Number
		Diameter (in.)	Density (g/cm <sup>3</sup> )		
19	5.2127	0.2175	9.8562	1.992	B-95
20	5.4919	0.2178	9.8314	1.992	B-95
21	5.7703	0.2178	9.8479	1.992	B-95
22	6.0508	0.2179	9.7768	1.992	B-95
23	6.3222	0.2172	9.7995	1.989	B-96
24	6.5947	0.2162	9.8993	1.983	B-96
25	6.8679	0.2164	9.8678	1.983	B-96
26	7.1420	0.2164	9.7688	1.983	B-96
27	7.4144	0.2166	9.8055	1.983	B-96
28	7.6884	0.2169	9.7696	1.983	B-96
29	7.9624	0.2160	9.8877	1.983	B-96
30	8.2364	0.2170	9.7726	1.983	B-96
31	8.5118	0.2170	9.7589	1.983	B-96
32	8.7851	0.2166	9.8339	1.983	B-96
33	9.0586	0.2169	9.8116	1.989	B-96
34	9.3326	0.2168	9.8088	1.989	B-96
35	9.6064	0.2168	9.8159	1.989	B-96
36	9.8808	0.2169	9.7975	1.989	B-96
37	10.1534	0.2172	9.8108	1.989	B-96
38	10.4269	0.2171	9.7996	1.989	B-96
39	10.6998	0.2171	9.8090	1.989	B-96
40	10.9720	0.2172	9.7949	1.989	B-96
41	11.2452	0.2171	9.8164	1.989	B-96
42	11.5189	0.2171	9.7864	1.989	B-96
43	11.7919	0.2172	9.7662	1.989	B-96
44	12.0652	0.2171	9.7404	1.989	B-96
45	12.3393	0.2169	9.7901	1.989	B-96
46	12.6133	0.2174	9.7487	1.989	B-96
47	12.8852	0.2173	9.7786	1.989	B-96
48	13.1576	0.2172	9.7635	1.989	B-96
49	13.4292	0.2170	9.8286	1.989	B-96
50	13.7042	0.2175	9.7043	1.989	B-96
51	13.9775	0.2174	9.7677	1.989	B-96
52	14.2500	0.2171	9.8113	1.989	B-96

## Annex II

## II. Irradiation Test Conditions [Elements PNL 3-30 (X-054) and PNL 5-31 (X-051)]

A. Irradiation Conditions

The following describes the irradiation test conditions for PNL 3-30 and PNL 5-31 irradiated in EBR-II in a 37-bare-pin subassembly. Although reactor power graphs can be supplied which average the reactor power over a 24-hr period, it is felt that data in this form would not satisfy the requirements of models which require knowledge of power cycles greater than a specified percent of full power operation. Although EBR-II maintains records showing the instantaneous power profile, these data are not presently available without a specific request from EBR-II.

Figures II.1 and II.2 give the linear power generation for PNL 3-30 and PNL 5-31, respectively, as a function of burnup. These data were calculated by R. E. Dahl from EBR-II estimated fission rates. Uncertainties are such that the power estimates are thought accurate to only +5%, -20%. The power levels were calculated from the following data:

Element PNL 3-30 - Loaded run 32B  
 Run missed 38A  
 Out estimated cycle 45 (end)  
 Position 3A2  
 Total calculated exposure -  
 15,302 Mwd/metric ton

Fluences shown in the data record are based upon accumulated megawatt second for PNL 3-30 to the end of run 45. All flux levels are based upon EBR-II reactor run 31F:

Total weight of mixed oxide, g	78.85
<sup>235</sup> U, % of total U	0.721
<sup>239</sup> Pu, % of total Pu	86.78
Pu content, wt %	21.8

The expected peak burnup is 27,270 Mwd/metric ton of metal assuming 50-MW reactor power and 309 full power days. The calculated fission rate at the start of irradiation was  $2.47 \times 10^{13}$  fissions  $\text{cm}^{-3} \text{sec}^{-1}$  and at 27,270 Mwd/metric ton, 2.95 at. % burnup, is expected to be  $2.304 \times 10^{13}$  fissions  $\text{cm}^{-3} \text{sec}^{-1}$  due to a 6.94% loss in power from burnout.

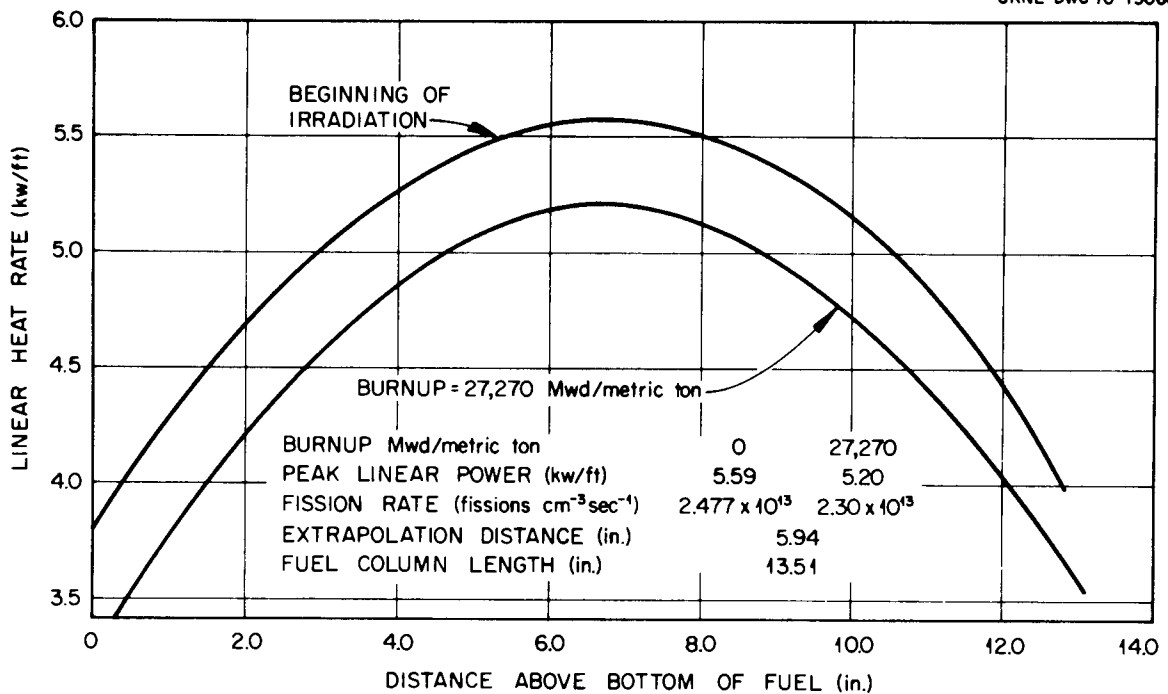


Fig. II.1. Linear Power as a Function of Axial Position for PNL 3-30.

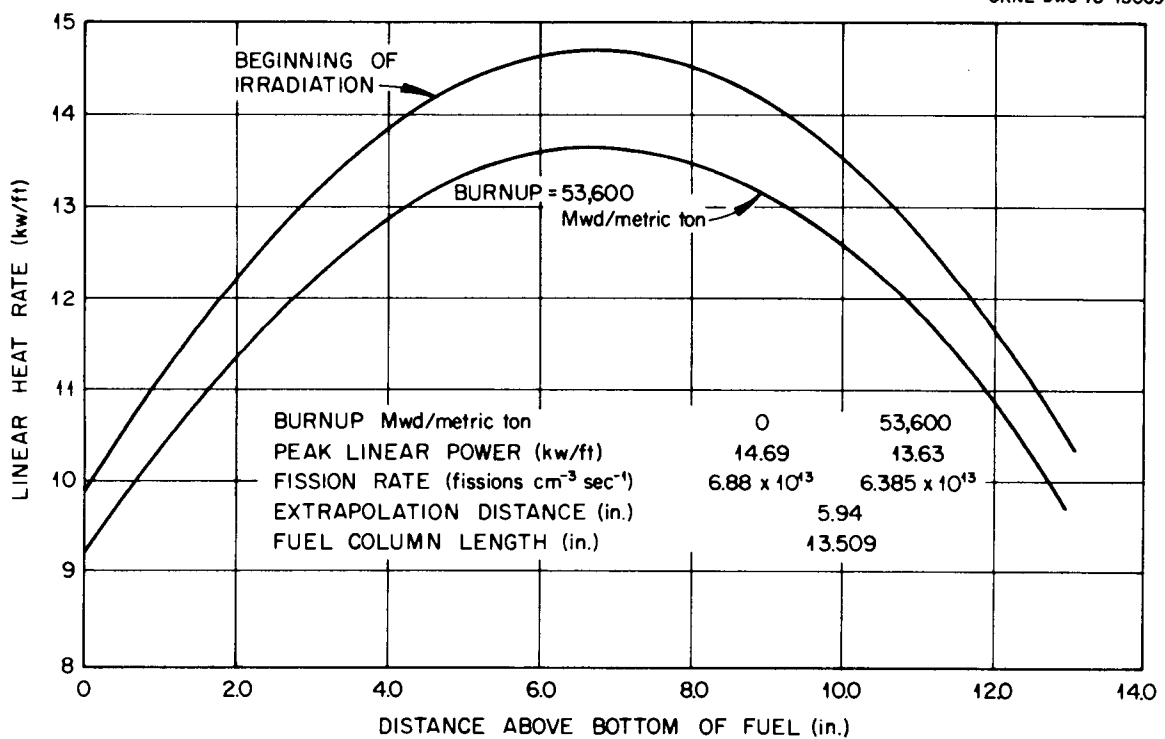


Fig. II.2. Linear Power as a Function of Axial Position for PNL 5-31.

Element PNL 5-31 - Loaded run 33B (3/31/69)  
 Position 4E1  
 Run missed 38A  
 Removed run 42 (5/18/70)  
 Total accumulated exposure -  
 11,107 MWd/metric ton

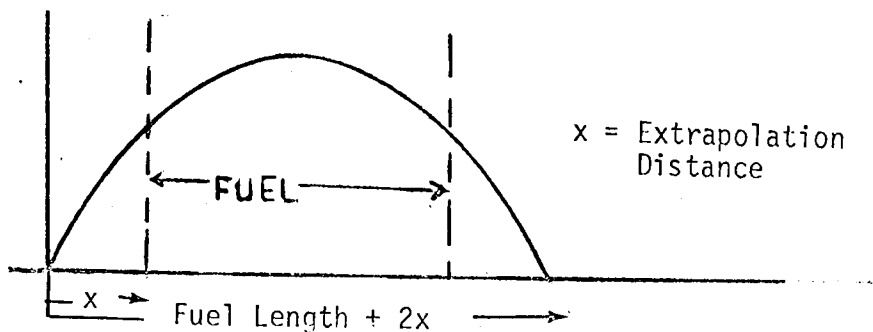
Flux estimates are based upon EBR-II reactor run 31F. Fluences are based upon accumulated megawatt second for PNL 5-31 reported by EBR-II.

Total weight of mixed oxide, g	78.74
$^{235}\text{U}$ and % of total U	93.12
$^{239}\text{Pu}$ and % Pu	86.135
Pu content, wt %	22.2

The expected burnup is 53,600 MWd/metric ton metal assuming a reactor power of 50 MW(t) and 222 full power days of irradiation. The calculated fission rate at the start of irradiation was  $6.88 \times 10^{13}$  fissions  $\text{cm}^{-3} \text{sec}^{-1}$  and at 53,000 MWd/metric ton, 6.68 at. % burnup, was  $6.39 \times 10^{13}$  fissions  $\text{cm}^{-3} \text{sec}^{-1}$  due to 7.12% loss in power from burnout.

#### Temperature Profiles

Figures II.3 and II.4 show the calculated axial cladding outer diameter temperature profiles at 50 MW(t). The sodium inlet temperature is shown for reference. The axial temperature profiles are generated with SINTER, a computer code written by Dick Shields to assess the temperature distribution in fuel elements. The data are based upon a sodium inlet temperature of 700°F and assume a chopped cosine power profile of the form



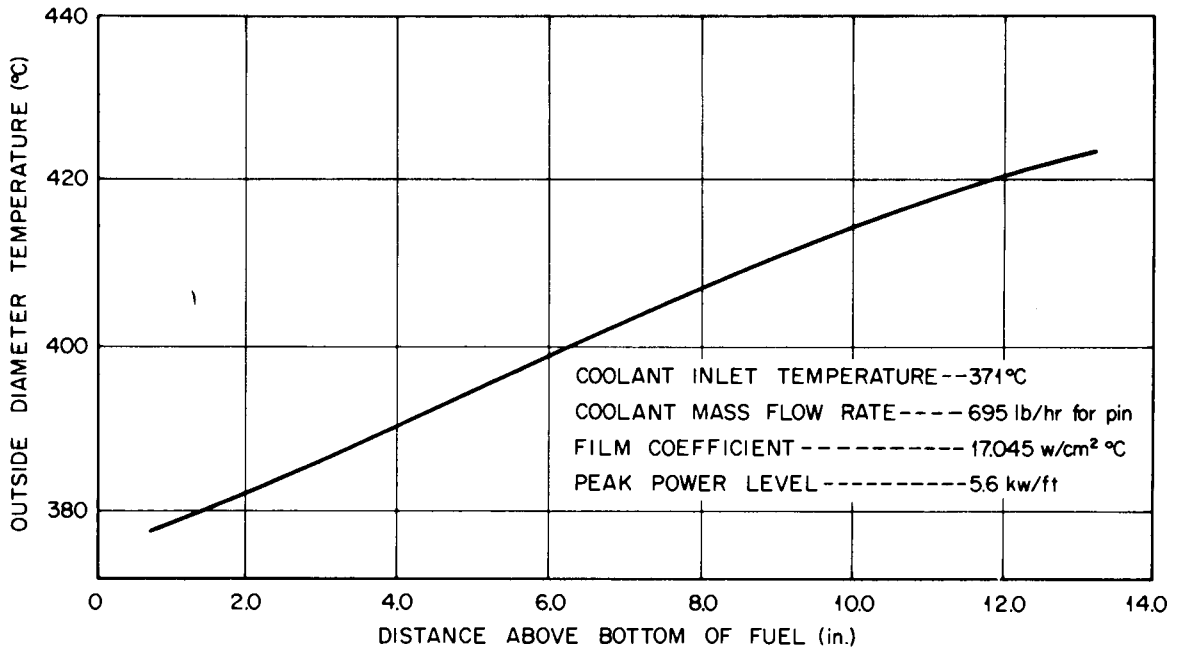


Fig. II.3. Axial Temperature Distribution at Cladding Surface for PNL 3-30.

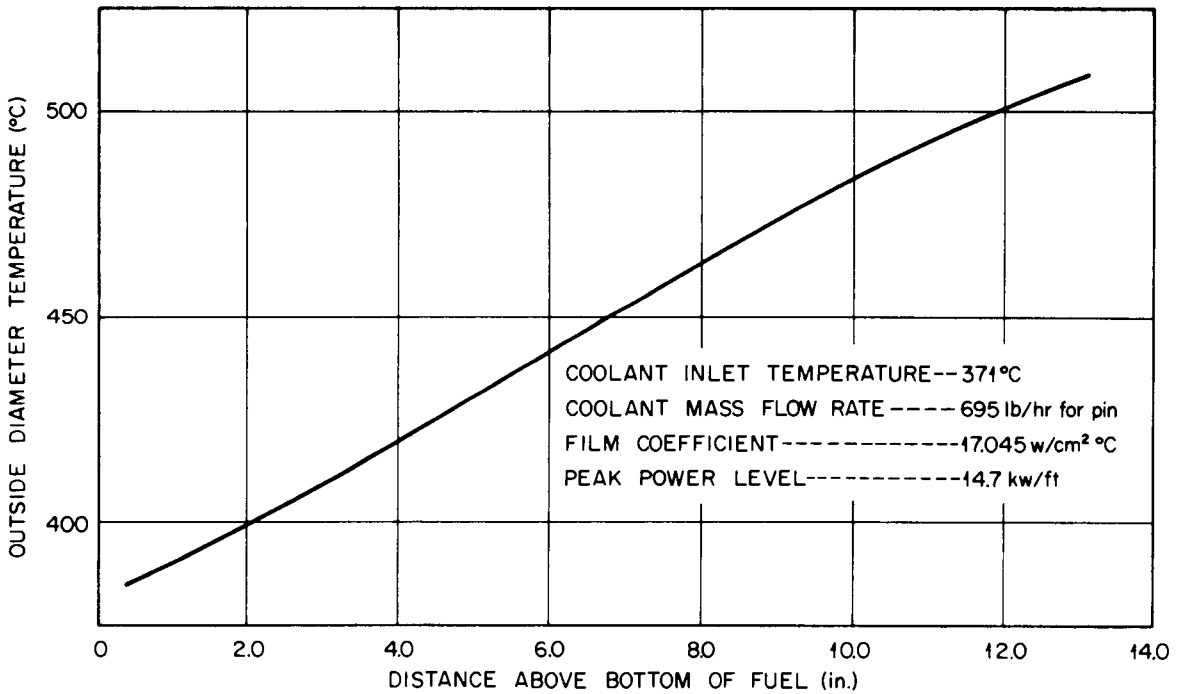


Fig. II.4. Axial Temperature Distribution at Cladding Surface for PNL 5-31.

Figures II.1 and II.2 show the calculated axial power profiles of the two pins. Uncertainties in the actual peak linear power create an uncertainty in the local power generation of +5, -20%.

### History

Since most of the time at power was accumulated at 50 MW(t), a reasonable approximation of the history can be obtained by dividing the accumulated megawatt days by 50 MW(t).

PNL 3-30 -  $15,302/50 = 306$  equivalent full power days

PNL 5-31 -  $11,107/50 = 222.5$  equivalent full power days

Computer cards showing the EBR-II approach to reactor power during runs 32B or 33B or for the entire power history (32B - 45, less 38A for PNL 3-30) and (33B - 42, less 38A for PNL 5-31) can be provided by request from L. Pember, Building 309, WADCO, Richland, Washington, or by direct contact with EBR-II.

### B. Burnup and Fluence Summary

<u>Capsule Identification</u>	<u>PNL 3-30</u>	<u>PNL 5-31</u>
Calculated peak burnup, MWd/metric ton	27,270	53,600
Assumed flux, neutrons $\text{cm}^{-2} \text{sec}^{-1}$	$1.95 \times 10^{15}$	$1.72 \times 10^{15}$
Calculated total fluences, neutrons/ $\text{cm}^2$ } ( > 0.1 MeV )	$5.15 \times 10^{22}$ $4.52 \times 10^{22}$	$3.311 \times 10^{22}$ $2.882 \times 10^{22}$

### C. Preirradiation Fuel Parameters

<u>Capsule Identification</u>	<u>PNL 3-30</u>	<u>PNL 5-31</u>
Fuel type	Solid pellet	Solid pellet
Pu content, wt % (average)	21.80	22.20
U content, wt % (average)	65.60	66.10
Pellet theoretical density, $\text{g}/\text{cm}^3$	11.01	10.88
Pellet density, % of theoretical	89.62-91.52	90.01-91.27
Mean density, % of theoretical	90.38	90.59
Stoichiometry, O:metal	1.97	1.95-1.96
Fuel weight, g	78.85	78.74

<u>Capsule Identification</u>	<u>PNL 3-30</u>	<u>PNL 5-31</u>
Length, in.	13.510	13.509
Mean pellet diameter, in.	0.2136	0.2136
Fuel-cladding gap, mils*	5.5-6.0	5.8-6.5

D. Preirradiation Cladding Parameters

<u>Cladding Identification</u>	<u>PNL 3-30</u>	<u>PNL 5-31</u>
Cladding, type stainless steel	304	304
Condition	Annealed	Annealed
Diameter, in.		
Inside	0.2193	0.2196
Outside	0.2505	0.2504
Nominal wall, mils	15.6	15.4

Additional information of cladding condition and physical properties is tabulated in Table II.3 of Appendix II.

The cladding was wrapped on the outside diameter with type 304 stainless steel wire  $62.5 \pm 0.5$  mils in diameter with a 12-in. pitch and was tack welded at each end of the pin.

---

\*Cold. Local gap can be calculated from individual pellet dimensions in Table II.2 of Appendix II.



APPENDIX II



Table II.1. Miscellaneous Preirradiation Information

Capsule Identification	PNL 3-30	PNL 5-31
Approximate plenum volume, cm <sup>3</sup>	7.17	7.17
Number of fuel pellets	54	52
Fuel volume, cm <sup>3</sup>	7.63	7.77
Average fuel smear density, g/cm <sup>3</sup>	9.44	9.39
Length of bottom insulator pellet, in.	0.506	0.501
Plenum gas	Helium	Helium
Plenum gas pressure (initial), psi	14.6	14.6

Table II.2(a) Pellet Dimensions and Local Density of Pin PNL 3-30

Ref. Measured	Outside Diameter (in.)		Length (in.)	Weight (g)	Fuel $\rho^a$ (g/cm <sup>3</sup> )	Smear $\rho^b$ (g/cm <sup>3</sup> )
0.0	0.2134	0.2136	0.2488	1.4694	10.0670	9.5416
	0.2137	0.2138	0.2509	1.4678	9.9486	9.4514
	0.2137	0.2137	0.2516	1.4640	9.8999	9.4007
	0.2136	0.2136	0.2474	1.4481	9.9679	9.4565
	0.2135	0.2140	0.2466	1.4479	9.9895	9.4858
	0.2134	0.2135	0.2528	1.4723	9.9320	9.4091
	0.2135	0.2136	0.2532	1.4754	9.9278	9.4141
	0.2136	0.2139	0.2533	1.4813	9.9450	9.4480
	0.2136	0.2136	0.2528	1.4700	9.9025	9.3944
	0.2135	0.2135	0.2478	1.4578	10.0278	9.5045
	0.2135	0.2135	0.2530	1.4739	9.9302	9.4120
	0.2137	0.2138	0.2491	1.4541	9.9270	9.4309
	0.2136	0.2136	0.2469	1.4453	9.9688	9.4573
	0.2134	0.2134	0.2515	1.4555	9.8740	9.3986
	0.2135	0.2136	0.2524	1.4718	9.9350	9.4209
	0.2135	0.2137	0.2500	1.4685	10.0032	9.4900
	0.2135	0.2137	0.2452	1.4218	9.8747	9.3680
	0.2136	0.2138	0.2563	1.4961	9.9314	9.4307
	0.2134	0.2135	0.2520	1.4643	9.9093	9.3877
	0.2134	0.2135	0.2490	1.4717	10.0794	9.5488
	0.2138	0.2139	0.2610	1.5429	10.0435	9.5505
	0.2136	0.2138	0.2529	1.4811	9.9640	9.4616
	0.2134	0.2134	0.2506	1.4568	9.9183	9.3918
	0.2135	0.2136	0.2522	1.4721	9.9449	9.4302
	0.2133	0.2134	0.2483	1.4566	10.0135	9.4775
	0.2136	0.2137	0.2508	1.4732	9.9985	9.5241
	0.2135	0.2136	0.2528	1.4650	9.8735	9.3625
	0.2135	0.2136	0.2474	1.4409	9.9230	9.4095
	0.2134	0.2136	0.2505	1.4505	9.8701	9.3549
	0.2136	0.2139	0.2474	1.4478	9.9519	9.4545
	0.2136	0.2136	0.2521	1.4646	9.8935	9.3859
	0.2135	0.2136	0.2514	1.4722	9.9772	9.4609
	0.2135	0.2136	0.2502	1.4584	9.9311	9.4172
	0.2135	0.2136	0.2502	1.4694	10.0060	9.4882
	0.2132	0.2134	0.2513	1.4602	9.9231	9.3875
	0.2134	0.2135	0.2477	1.4494	9.9788	9.4535
	0.2135	0.2138	0.2464	1.4316	9.8897	9.3867
	0.2132	0.2135	0.2501	1.4586	9.955	9.4222
	0.2135	0.2135	0.2472	1.4387	9.9205	9.4027
	0.2139	0.2137	0.2497	1.4552	9.906	9.4153
	0.2134	0.2134	0.2503	1.4531	9.905	9.3792
	0.2137	0.2138	0.2489	1.4510	9.9138	9.4183
	0.2133	0.2133	0.2448	1.4218	9.9187	9.3833
	0.2134	0.2135	0.2448	1.4231	9.9138	9.3919

Table II.2(a) (continued)

Ref. Measured	Outside Diameter (in.)	Length (in.)	Weight (g)	Fuel $\rho^a$ (g/cm <sup>3</sup> )	Fuel $\rho^b$ (g/cm <sup>3</sup> )	
	0.2135	0.2135	0.2508	1.4627	9.9412	9.4223
	0.2133	0.2136	0.2470	1.4392	9.9366	9.4136
	0.2139	0.2138	0.2479	1.4490	9.9307	9.4433
	0.2136	0.2139	0.2481	1.4668	10.054	9.5516
	0.2138	0.2138	0.2496	1.4700	10.0107	9.5149
	0.2134	0.2137	0.2455	1.4444	10.0241	9.5053
	0.2136	0.2134	0.2448	1.4390	10.0199	9.4969
	0.2135	0.2137	0.2512	1.4787	10.0246	9.5102
	0.2137	0.2137	0.2493	1.4658	10.0078	9.5032
13.51	0.2136	0.2136	0.2499	1.4655	9.9911	9.4785
Average value					9.9954	9.44245

<sup>a</sup>Using dimensional and weight measurements shown for right circular cylinder.

<sup>b</sup>Based on cladding inside diameter = 0.2193.

Table II.2(b) Pellet Dimensions and Local Density of Pin PNL 5-31

Ref. Measured	Outside Diameter (in.)		Length (in.)	Weight (g)	Fuel $\rho^a$ (g/cm <sup>3</sup> )	Smear $\rho^b$ (g/cm <sup>3</sup> )
0.0	0.2134	0.2135	0.2525	1.4716	9.9429	9.3939
	0.2139	0.2138	0.2589	1.5124	9.9249	9.4119
	0.2134	0.2135	0.2525	1.4646	9.8918	9.3455
	0.2135	0.2136	0.2529	1.4781	9.9578	9.4167
	0.2135	0.2135	0.2608	1.5257	9.9948	9.4255
	0.2136	0.2139	0.2630	1.5279	9.8795	9.3601
	0.2139	0.2138	0.2586	1.5129	9.9397	9.4259
	0.2136	0.2136	0.2606	1.5180	9.9198	9.3851
	0.2137	0.2135	0.2578	1.5043	9.9370	9.4014
	0.2134	0.2134	0.2585	1.5036	9.9241	9.3789
	0.2133	0.2135	0.2700	1.5736	9.9437	9.3902
	0.2137	0.2136	0.2661	1.5528	9.9328	9.4019
	0.2137	0.2139	0.2662	1.5576	9.9458	9.4274
	0.2134	0.2135	0.2629	1.5424	10.0051	9.4526
	0.2135	0.2134	0.2575	1.5002	9.9355	9.3867
	0.2137	0.2137	0.2603	1.5169	9.9147	9.3891
	0.2134	0.2133	0.2574	1.4925	9.8976	9.3422
	0.2136	0.2136	0.2583	1.5015	9.8993	9.3658
	0.2136	0.2135	0.2542	1.4793	9.9149	9.3761
	0.2136	0.2139	0.2595	1.5079	9.8817	9.3622
	0.2134	0.2134	0.2678	1.5602	9.9400	9.3867
	0.2135	0.2134	0.2545	1.4773	9.8991	9.3524
	0.2136	0.2136	0.2665	1.5510	9.9111	9.3769
	0.2134	0.2134	0.2587	1.5008	9.8980	9.3469
	0.2137	0.2136	0.2654	1.5558	9.9783	9.4449
	0.2135	0.2134	0.2597	1.5242	10.0089	9.4561
	0.2137	0.2136	0.2602	1.5125	9.8944	9.3655
	0.2137	0.2137	0.2627	1.5387	9.9654	9.4371
	0.2136	0.2135	0.2589	1.5135	9.9600	9.4188
	0.2134	0.2135	0.2596	1.5025	9.8702	9.3251
	0.2134	0.2136	0.2686	1.5766	10.0052	9.4571
	0.2135	0.2133	0.2521	1.4638	9.9067	9.3552
	0.2136	0.2136	0.2674	1.5637	9.9586	9.4218
	0.2139	0.2137	0.2635	1.5338	9.8942	9.3785
	0.2136	0.2137	0.2521	1.4654	9.8943	9.3654
	0.2135	0.2136	0.2567	1.4986	9.9467	9.4060
	0.2138	0.2138	0.2544	1.4854	9.9247	9.4074
	0.2134	0.2135	0.2657	1.5529	9.9671	9.4166
	0.2136	0.2136	0.2664	1.5540	9.9340	9.3985
	0.2135	0.2137	0.2615	1.5350	9.9964	9.4576
	0.2136	0.2137	0.2450	1.4231	9.8872	9.3586
	0.2134	0.2136	0.2478	1.4382	9.8930	9.3511
	0.2133	0.2135	0.2579	1.4946	9.8876	9.3372

Table II.2(b) (continued)

Ref. Measured	Outside Diameter (in.)		Length (in.)	Weight (g)	Fuel $\rho^a$ (g/cm <sup>3</sup> )	Fuel $\rho^b$ (g/cm <sup>3</sup> )
	0.2136	0.2135	0.2641	1.5478	9.9852	9.4426
	0.2134	0.2135	0.2677	1.5607	9.9423	9.3932
	0.2134	0.2135	0.2604	1.5245	9.9839	9.4326
	0.2132	0.2134	0.2644	1.5409	9.9527	9.3898
	0.2137	0.2138	0.2636	1.5421	9.9486	9.4256
	0.2137	0.2136	0.2575	1.5036	9.9393	9.4080
	0.2137	0.2138	0.2509	1.4605	9.8991	9.3787
	0.2131	0.2131	0.2612	1.5167	9.9350	9.3556
13.51	0.2133	0.2132	0.2581	1.4923	9.8787	9.3156
	Average value				9.9331	9.3931
	1 $\sigma$				0.0369	0.03724

<sup>a</sup>Using dimensional and weight measurements shown for right circular cylinder.

<sup>b</sup>Based on cladding inside diameter = 0.2196.

Table II.3. Cladding Condition and Physical Properties<sup>a</sup>

<u>Cold-Work Method</u>			
	<u>Annealing Temperature (°C)</u>	<u>Reduction (%)</u>	
Sinking	1066	25	
Draw	1066	23	
Draw	1066	0	
Sinking	1066	16	
Final anneal, 1066°C			
<u>Machine-Straightened Tubing</u>			
<u>Property<sup>b</sup></u>	<u>Temperature</u>	<u>Value</u>	<u>Unit</u>
0.2% yield	427°C	23.56, 23.31, 23.56	ksi
0.2% yield	538°C	22.46, 25.42, 23.22	ksi
Uniform elongation	427°C	36.35, 37.79, 32.70	%
Total elongation	427°C	42.00, 42.65, 34.90	%
Uniform elongation	538°C	36.67, 37.79, 32.70	%
Total elongation	538°C	45.45, 40.90, 42.26	%
Strain hardening <sup>c</sup>	427°C	0.3101, 0.3206, 0.2829	
Coefficient	538°C	0.3124, 0.3081, 0.3111	

<sup>a</sup>These data are suitable for both PNL 3-30 and PNL 5-31.

<sup>b</sup>Data at strain rate of 0.01/min.

<sup>c</sup>Slope of plastic portion of true stress-true strain curve.

Table II.4. Starting Fuel Isotopic Content

Capsule Identification	PNL 3-30	PNL 5-31
Uranium	% of total U	
234	0.006	0.514
235	0.721	93.12
236		0.323
238	99.273	6.04
Plutonium	% of total Pu	
238	0.036	0.065
239	86.78	86.185
240	11.54	11.297
241	1.51	2.259
242	0.003	0.194
Fuel impurities, ppm		
Al	50	50
Fe	50	20
Ni	20	20
C	50	60
Ca	50	10
Cr	25	25
Cl	10	10
Na		2.0
Fl		5.0

## Annex III

III. LMFBR Demonstration Plant

The following two hypothetical fuel problems were supplied by Atomics International as representative of conditions in the Liquid Metal Fast Breeder Reactor Demonstration Plant. The two cases are identical except for differences in fuel density. Table III.1 shows the design parameters. Table III.2 shows the axial power profile and cladding temperature.

Table III.1. Design Parameters for Demonstration  
Plant Checkout Problem

Cladding material	Type 316 stainless steel 20% cold worked
Cladding outside diameter, in.	0.300
Cladding thickness, in.	0.0180
PuO <sub>2</sub> fraction	24.5%
Fuel pellet diameter, in.	0.2580
O:metal ratio	1.96
Fuel pellet fabricated density	
80% smear density	83.764% theoretical
85% smear density	89.000% theoretical
Active fuel length, in.	51.1
Plenum length, in.	30.0
Helium fill pressure at 70°F,	1.0 atm
Sodium coolant velocity, ft/sec	30.5
Total fluence at 100,000 MWd/ metric ton peak burnup, neutrons/cm <sup>2</sup>	$4.135 \times 10^{23}$
Total fast fluence (> 1.0 MeV) at 100,000 MWd/metric ton peak burnup, neutrons/cm <sup>2</sup>	$4.135 \times 10^{22}$
Reactor shutdowns to 0 power for refueling at following burnup, MWd/metric ton	25,000 50,000 75,000 100,000

Table III.2. Linear Power and Outside Diameter Cladding Temperature for Eleven Equally Spaced Fuel Nodes

Node <sup>a</sup>	kW/ft	Cladding Temperature	
		(°F)	(°C)
1	5.864	777	414
2	8.904	802	428
3	11.485	835	446
4	13.389	873	467
5	14.592	912	489
6	15.000	952	511
7	14.592	991	533
8	13.389	1027	553
9	11.458	1056	569
10	8.904	1080	582
11	5.864	1094	590
Plenum	0.0	1094	590

<sup>a</sup>Integral axial blanket regions are assumed to generate negligible power and to contribute negligible void volume for fission gas storage.

## Annex IV

IV. ORNL Power Cycle Test

The last problem is the Oak Ridge MINT-2 irradiation experiment which is designed to study the effect of reactor power changes on fuel performance. The experiment will be initiated as a programmed power cycling test in the ORR poolside facility during FY 1971. It will be instrumented to measure cladding temperature and fuel and cladding axial deformation.

A. Irradiation Test Conditions

As currently planned, the initial increase to power from 0 to 16 kW/ft will occur in steps of 1.6 kW/ft in 3-hr intervals every other day (or about a 20-day startup period). Subsequent operation will be as shown in Fig. IV.1. The relative power of 1.0 corresponds to 16 kW/ft. "Occasional overpower" operating conditions will also occur which will give peak linear power of 19 kW/ft and a peak outer surface temperature of 660°C. Operation will last about 8000 hr to approximately 8.5 at. % burnup of initial heavy atoms.

B. Calculated Linear Power and Cladding Temperature

Table IV.1 shows the axial power profile, outside cladding temperature, and cladding neutron flux as a function of length. The axial power profile and cladding temperature are for overpower conditions when the external coolant pressure is 60 psi and the plenum temperature is 130°C.

Since irradiation will occur in a thermal flux, Fig. IV.2 shows the calculated radial power density in the fuel as a function of burnup.

The calculated variation in cladding neutron flux with burnup is shown in Table IV.2.

C. Design Fabrication Data

Table IV.3 shows the fabrication data for the MINT-2 experiment. Note that the pin has 9.6 in. of mixed oxide fuel in the center and 0.2 in. of UO<sub>2</sub> representing an axial blanket in each end of the fuel column.

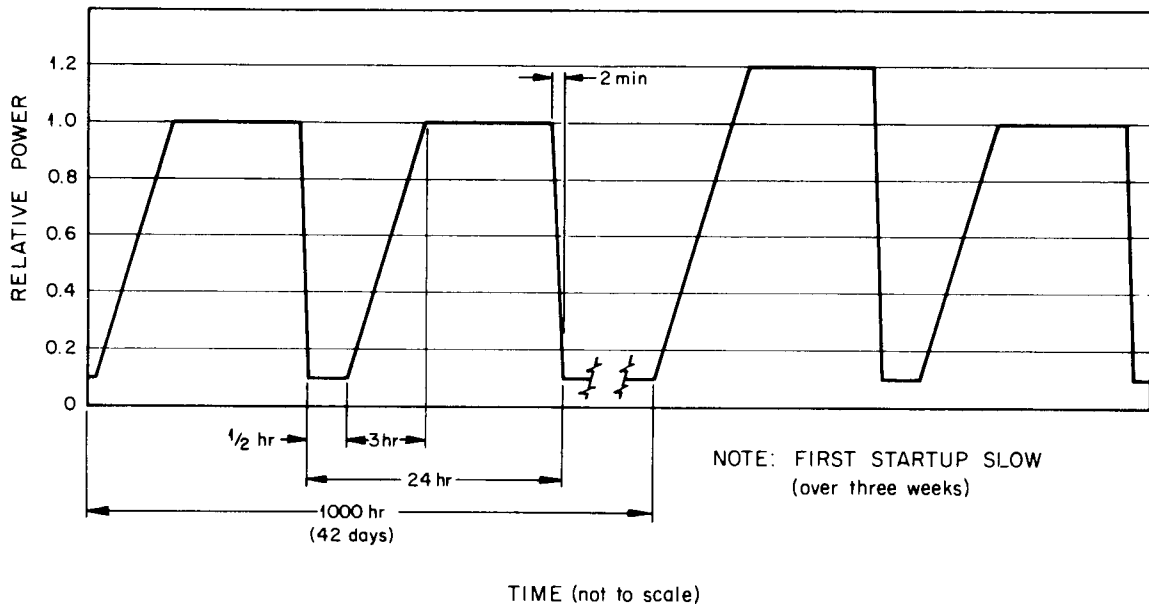


Fig. IV.1. Proposed Shape of Power Cycles.

Table IV.1. Operating Conditions for MINT-2 Capsule at Overpower Conditions<sup>a,b</sup>

Axial Position (z/z <sub>0</sub> )	Heat Rate (kW/ft)	Cladding Outer Surface Temperature (°C)	Cladding Neutron Flux at Startup [neutrons cm <sup>-2</sup> sec <sup>-1</sup> (> 0.1 MeV)]
			× 10 <sup>13</sup>
0	15.31	513	1.21
0.1	16.15	535	1.28
0.2	17.00	559	1.34
0.3	17.81	581	1.41
0.4	18.62	604	1.47
0.5	19.00	615	1.50
0.6	18.62	604	1.47
0.7	17.81	581	1.41
0.8	17.00	559	1.34
0.9	16.15	535	1.28
1.0	15.31	513	1.21

<sup>a</sup> External coolant pressure = 60 psi.

<sup>b</sup> Gas plenum temperature exterior to fuel region = 130°C.

<sup>c</sup> Temperature profile is symmetrical about the center as specimens are conductively cooled in the ORR pool. Temperatures for other power conditions can be estimated by ratioing the temperature drop (value shown - 130°C) to the power levels desired.

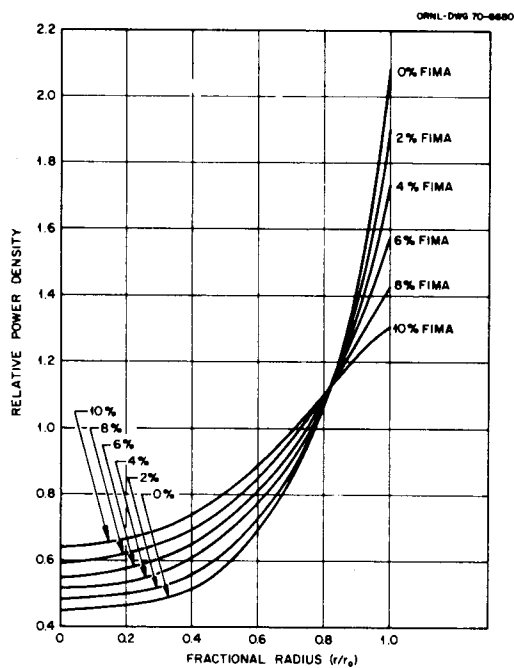


Fig. IV.2. Effect of Burnup on Fuel Radial Power Profile - MINT Capsule.

Table IV.2. Variation of Cladding Neutron Flux with Burnup

Burnup (% FIMA)	Neutron Flux [neutrons $\text{cm}^{-2} \text{sec}^{-1}$ ( $> 0.1 \text{ MeV}$ )]
	$\times 10^{13}$
0	1.50
2	1.54
4	1.57
6	1.61
8	1.66
10	1.71

Table IV.3. Design Fabrication Data for MINT-2 Experiment

Fuel composition	$U_{0.75}Pu_{0.25}O_{1.98}$
Fuel fabrication form	Solid pellets with flat, square ends and $L/D = 1$
Fuel pellet diameter, in.	0.198
Fuel pellet density, % of theoretical	92
Fuel grain size, $\mu m$	10
Fuel column length, in.	9.6
Axial blanket composition	$UO_2$
Blanket fabrication form	Solid pellets with flat, square ends and $L/D = 1$
Blanket pellet diameter, in.	0.194
Blanket pellet density, % of theoretical	95
Blanket length, in., each end	0.2
Fuel axial restraint	Spring loaded to 1 1/4 lb with 9.8 lb/in. spring constant
Fuel-to-cladding bond	1 atm He at 24°C
Gas plenum volume exterior to fuel region, $cm^3$ STP	5
Cladding material	20% cold-worked type 316 stainless steel
Cladding outside diameter, in.	0.230
Cladding wall thickness, in.	0.015
Fuel pin coolant	Stagnant NaK-44

•

•

•

•

•

•

## INTERNAL DISTRIBUTION

- |       |                               |        |                 |
|-------|-------------------------------|--------|-----------------|
| 1-3.  | Central Research Library      | 23.    | J. H Frye, Jr.  |
| 4.    | ORNL - Y-12 Technical Library | 24.    | W. O. Harms     |
|       | Document Reference Section    | 25-27. | M. R. Hill      |
| 5-14. | Laboratory Records Department | 28-32. | F. J. Homan     |
| 15.   | Laboratory Records, ORNL-RC   | 33.    | W. J. Lackey    |
| 16.   | ORNL Patent Office            | 34.    | A. L. Lotts     |
| 17.   | G. M. Adamson, Jr.            | 35.    | A. R. Olsen     |
| 18.   | C. M. Cox                     | 36.    | P. Patriarca    |
| 19.   | F. L. Culler, Jr.             | 37.    | J. L. Scott     |
| 20.   | J. E. Cunningham              | 38.    | D. B. Trauger   |
| 21.   | R. B. Fitts                   | 39.    | T. N. Washburn  |
| 22.   | M. Fontana                    | 40.    | J. R. Weir, Jr. |

## EXTERNAL DISTRIBUTION

41. W. J. Anderson, Atomics International, P. O. Box 309, Canoga Park, CA 91304
42. W. E. Baily, General Electric Company, BRDO, Sunnyvale, CA 94086
43. C. J. Baroch, Babcock & Wilcox Company, P. O. Box 1260, Lynchburg, VA 24505
44. A. Bauer, Battelle Memorial Institute, 505 King Avenue, Columbus, OH 43201
45. A. Boltax, Westinghouse Electric Corporation, Waltz Mill Site, P. O. Box 158, Madison, PA 15663
46. H. L. Brown, AEC, Washington, DC 20545
47. W. E. Burchill, Combustion Engineering, 1000 Prospect Hill Rd., Windsor, CT 06095
- 48-49. E. G. Case, Director, Division of Reactor Standards, AEC, Washington, DC 20545
50. D. F. Cope, RDT, SSR, AEC, Oak Ridge National Laboratory
51. J. B. Dee, Gulf General Atomic, P. O. Box 608, San Diego, CA 92112
52. R. C. Erdman, Associate Professor, Energy and Kinetics Department, School of Engineering and Applied Science, UCLA, Los Angeles, CA 90024
53. E. A. Evans, WADCO, P. O. Box 1970, Richland, WA 99352
54. F. Gelhaus, General Electric Company, Sunnyvale, CA 94086
55. G. Golden, Argonne National Laboratory, 9700 South Cass Avenue, Argonne, IL 60439
56. Sam P. Grant, Nuclear Power Generation Department, Lynchburg, VA 24505
57. J. Green, Los Alamos Scientific Laboratory, P. O. Box 1663, Los Alamos, NM 87544
58. B. Harbourne, Westinghouse Electric Corporation, Waltz Mill Site, P. O. Box 158, Madison, PA 15663
59. D. P. Hines, General Electric Company, BRDO, Sunnyvale, CA 94086

60. R. J. Jackson, WADCO, P. O. Box 1970, Richland, WA 99352
61. D. L. Keller, Battelle Memorial Institute, 505 King Avenue, Columbus, OH 43201
62. E. E. Kintner, RDT, AEC, Washington, DC 20545
63. M. Marlow, General Electric Company, Vallecitos Nuclear Center, P. O. Box 846, Pleasanton, CA 94566
64. C. L. Matthews, RDT, OSR, AEC, Oak Ridge National Laboratory
65. W. Meinhardt, General Electric Company, Sunnyvale, CA 94086
66. A. C. Millunzi, AEC, Washington, DC 20545
- 67-69. P. A. Morris, Director, Division of Reactor Licensing, AEC, Washington, DC 20545
70. P. Murray, Westinghouse Electric Corporation, Waltz Mill Site, P. O. Box 158, Madison, PA 15663
71. M. Nathan, Atomics International, P. O. Box 309, Canoga Park, CA 91304
72. E. C. Norman, RDT, AEC, Washington, DC 20545
73. D. Okrent, Department of Nuclear Engineering, University of Arizona, Tucson, AZ 85721
74. H. Pearlman, Atomics International, P. O. Box 309, Canoga Park, CA 91304
75. R. Propel, Argonne National Laboratory, 9700 South Cass Avenue, Argonne, IL 60439
76. W. E. Ray, Westinghouse Electric Corporation, Waltz Mill Site, P. O. Box 158, Madison, PA 15663
77. S. Rosen, RDT, AEC, Washington, DC 20545
78. F. Rough, Argonne National Laboratory, 9700 South Cass Avenue, Argonne, IL 60439
79. D. Sheibley, NASA, Lewis Research Center, Plum Brook Station, Taylor Road and Columbus Avenue, Sandusky, OH 44870
80. P. G. Shewmon, Argonne National Laboratory, 9700 South Cass Avenue, Argonne, IL 60439
81. S. Siegel, Atomics International, P. O. Box 309, Canoga Park, CA 91304
82. J. M. Simmons, RDT, AEC, Washington, DC 20546
83. A. A. Strasser, United Nuclear Corporation, Grasslands Rd., Elmsford, NY 10523
84. L. Tripp, NUS Corporation, 4 Research Place, Rockville, MD 20850
85. Arkira Watanabe, Argonne National Laboratory, 9700 South Cass Avenue, Argonne, IL 60439
86. C. E. Weber, RDT, AEC, Washington, DC 20546
87. R. W. Weeks, Argonne National Laboratory, 9700 South Cass Avenue, Argonne, IL 60439
88. Laboratory and University Division, AEC, Oak Ridge Operations
- 89-90. Division of Technical Information Extension